nature medicine

LETTERS

https://doi.org/10.1038/s41591-019-0371-0

Altered neuronal migratory trajectories in human cerebral organoids derived from individuals with neuronal heterotopia

Johannes Klaus[1,11], Sabina Kanton[2,11], Christina Kyrousi[1,11], Ane Cristina Ayo-Martin[1,3], Rossella Di Giaimo[1,4], Stephan Riesenberg[2], Adam C. O'Neill[5,6], J. Gray Camp[2], Chiara Tocco[1], Malgorzata Santel[2], Ejona Rusha[7], Micha Drukker[7], Mariana Schroeder[1], Magdalena Götz[6,8], Stephen P. Robertson[5], Barbara Treutlein[2,9,10*] and Silvia Cappello[1*]

Malformations of the human cortex represent a major cause of disability[1]. Mouse models with mutations in known causal genes only partially recapitulate the phenotypes and are therefore not unlimitedly suited for understanding the molecular and cellular mechanisms responsible for these conditions[2]. Here we study periventricular heterotopia (PH) by analyzing cerebral organoids derived from induced pluripotent stem cells (iPSCs) of patients with mutations in the cadherin receptor–ligand pair *DCHS1* and *FAT4* or from isogenic knockout (KO) lines[1,3]. Our results show that human cerebral organoids reproduce the cortical heterotopia associated with PH. Mutations in *DCHS1* and *FAT4* or knockdown of their expression causes changes in the morphology of neural progenitor cells and result in defective neuronal migration dynamics only in a subset of neurons. Single-cell RNA-sequencing (scRNA-seq) data reveal a subpopulation of mutant neurons with dysregulated genes involved in axon guidance, neuronal migration and patterning. We suggest that defective neural progenitor cell (NPC) morphology and an altered navigation system in a subset of neurons underlie this form of PH.

Mammalian neocortical development represents a highly orchestrated process that depends on the precise generation, migration and maturation of neurons. The importance of a coordinated sequence is underlined by the conditions with its disruption: malformation of cortical development. PH represents one of the most common forms of these disorders and is characterized by heterotopic neurons lining their sites of production. Patients with PH typically present with intellectual disability, and this is frequently associated with epilepsy[4–10]. The identification of mutations in the protocadherins *DCHS1* and *FAT4* put the spotlight on defects in NPCs as a causal mechanism of the condition. Here we explore the functions of DCHS1 and FAT4 in the developing cortex using human iPSC-derived NPCs, neurons and cerebral organoids.

We first reprogrammed fibroblasts from control individuals and patients with PH who carry mutations in *DCHS1* or *FAT4* into iPSCs (Extended Data 1a,b). Specifically, fibroblasts were collected from two different previously characterized patients[1,3]: one was compound heterozygous for mutations in the *FAT4* gene and one homozygous for mutation in the *DCHS1* gene. Additionally, to control for differences due to the different genomic background in the patients, we generated KO iPSC lines for both genes using CRISPR–Cas9 genome editing in control iPSCs. We programmed the iPSCs toward NPCs and neurons in two-dimensional (2D) culture and generated three-dimensional (3D) cerebral organoids[11] (Extended Data 1c,d). Using in situ hybridization, we identified that both genes were expressed in the periventricular structures of cerebral organoids and neurons (Extended Data 1e–h′), a pattern consistent with that detected in mouse and human[1,12]. These findings were confirmed by scRNA-seq of cells derived from cerebral organoids, where the expression of *DCHS1* and *FAT4* was found in both progenitors and neurons (Extended Data 1i,j).

To investigate whether PH is recapitulated within cerebral organoids (Extended Data 1k,l), we scrutinized ventricular zone structures for such phenotypes. In control organoids, a clear distinction of the neuronal (MAP2+ cells or NEUN+ cells) layer from the germinal zone (PAX6+ cells) was identified (Fig. 1a,d, Extended Data 2a,e,h and Extended Data 3g,k). Organoids derived from mutant or KO iPSC lines exhibited a significant number of neuronal nodules at ventricular positions (Fig. 1a–c, Extended Data 2e–j, and Extended Data 2l–l′′′). In addition to this neuronal heterotopia-like phenotype, mutant and KO organoids presented poorly organized germinal zones (Fig. 1d,e and Extended Data 2d). This feature was especially apparent in germinal zones of *FAT4*-mutant organoids, with most not showing evident separation of the neuronal band from the germinal zone, with neurons intruding in most cases. In the case of *DCHS1*-mutant or knockdown organoids, performed via electroporation of specifically designed microRNAs (miRNAs) that target the human gene (Extended Data 2k), clusters of neurons were found within the germinal zones where NPC processes where disrupted (Fig. 1f–f′′′ and Extended Data 2l–l′′′). Although *DCHS1*-mutant organoids displayed clearer separations between the germinal zones and neuronal layer, the neurites showed an

[1]Max Planck Institute of Psychiatry, Munich, Germany. [2]Max Planck Institute for Evolutionary Anthropology, Leipzig, Germany. [3]International Max Planck Research School for Translational Psychiatry (IMPRS-TP), Munich, Germany. [4]Department of Biology, University of Naples Federico II, Naples, Italy. [5]Department of Women's and Children's Health, University of Otago, Dunedin, New Zealand. [6]Institute of Stem Cell Research, Helmholtz Center Munich, Munich, Germany. [7]Institute of Stem Cell Research, iPSC Core Facility, Helmholtz Center Munich, Munich, Germany. [8]Ludwig Maximilian University, Munich, Germany. [9]Max Planck Institute of Molecular Cell Biology and Genetics, Dresden, Germany. [10]Technical University Munich, Department of Biosciences, Freising, Germany. [11]These authors contributed equally: Johannes Klaus, Sabina Kanton, Christina Kyrousi. *e-mail: barbara_treutlein@eva.mpg.de; silvia_cappello@psych.mpg.de

altered morphology compared with controls, with many processes appearing as thick bundles (Extended Data 2m–o). These findings show that cerebral organoids recapitulate the hallmarks of PH. The loss of organization (germinal zone versus cortical plate) in mutant organoids starts early, after 20 d of cerebral organoid development (Extended Data 3a–f), even though the sizes of the two zones (VZ and CP) are not altered (Extended Data 3g–j).

In mice, knockdown of *Dchs1* or *Fat4* leads to overproliferation of progenitors[1]. This increase in proliferation was not observed in human organoids derived from patient iPSCs (Extended Data 3k–s), highlighting fundamental species-specific differences. We analyzed the morphology of the processes of NPCs in organoids by NESTIN immunostaining in mutant or KO organoids. Whereas in control organoids the processes appeared to be aligned and straight, in *FAT4*-mutant or KO organoids, these processes were often disrupted and exhibited a twisted morphology (Fig.1g,i,m and Extended Data 4a,c). NPC morphology in *DCHS1*-mutant or KO organoids was less severely compromised (Fig.1g–i,m and Extended Data 4a–c). To scrutinize the morphology of single NPCs, we electroporated a Gap43-GFP plasmid[13] to label the cell membrane in mutant organoids. Analysis 4 d after electroporation showed that *FAT4*-mutant organoids had disrupted progenitor morphology (Fig.1j,l,n). Consistent with previous results, this phenotype was also observed in *DCHS1*-mutant organoids (Fig.1j,k,n).

To ensure that the observed phenotypic differences are not caused by the different genetic backgrounds of the cells of origin, we respectively and selectively knocked down *DCHS1* and *FAT4* in NPCs via electroporation of miRNAs in control organoids. 7 d post electroporation, we similarly observed a disruption in the morphology of NPCs upon *DCHS1* and *FAT4* knockdown (Fig. 1o and Extended Data 4d–f), suggesting that the morphology of NPCs is disturbed in organoids derived from cells with mutations or reduced *DCHS1* and *FAT4*.

Dchs1 and Fat4 have been described to localize apically and to form a heterophilic complex in the developing mouse brain[12]. We therefore hypothesized that DCHS1 and/or FAT4 could be key molecules in the maintenance of the polarity of NPCs. We found mislocalization of cilia labeled by ARL13B (Extended Data 5r), but the total proportion of apical and basal cilia was not altered (Extended Data 5p–s); in *FAT4*-mutant germinal zones and, to some extent, in *DCHS1*-mutant germinal zones, the apical surface exhibited a disrupted or discontinuous morphology with increased distance between the apical surface and the NPCs (Extended Data 5f–o). This finding further underlined that the defects in NPCs are more pronounced in *FAT4*-mutant organoids, but it also revealed that both mutations do not preclude the establishment of apicobasal polarity. To evaluate whether cytoskeletal dynamics are affected and possibly contributing to the disrupted morphology of NPCs in the patient-derived organoids, we performed immunohistochemistry for ACETYLATED TUBULIN, which labels stable microtubules. While the stable microtubules were not strongly affected in *DCHS1*-mutant NPCs, *FAT4*-mutant NPCs showed not only decreased organization but also markedly diminished levels of stable ACETYLATED TUBULIN (Extended Data 5a–c). To specifically detect levels of stable microtubules in NPCs, we performed a western blot analysis of ACETYLATED TUBULIN in NPCs from monolayer cultures and detected a significant decrease in ACETYLATED TUBULIN in *FAT4*-mutant NPCs. In contrast, TYROSINATED TUBULIN, which reflects the more dynamic form of tubulin, was not altered (Extended Data 5d,e).

In order to gain deeper insight into the molecular changes in progenitors and neurons of *DCHS1* and *FAT4* organoids, we next performed scRNA-seq to dissect the cell composition and transcriptional landscapes in *DCHS1*, *FAT4* and control (CTRL) organoids. We analyzed 805 single cells from three microdissected organoid cortical regions for each condition (nine organoids in total; 50–60 d) and identified progenitors and neurons based on known marker genes (Fig. 2a,b). In an unbiased principal component analysis (PCA), the first two components separate NPCs (e.g. *VIM*, *PAX6*, *SOX2*, *HES1*) and neurons (e.g. *DCX*, *STMN2*, *TUBB3*, *SNAP25*, *MYT1L*) independent of the condition (control, *DCHS1*, *FAT4*) (Fig. 2a,b and Supplementary Table 1). However, the third principal component segregates control cells from *DCHS1*- and *FAT4*-mutant cells, which remarkably intermingle, suggesting that cells derived from patients with mutation in *DCHS1* and *FAT4* share common transcriptome features distinct from the control cells (Fig. 2c). Interestingly, among the genes upregulated in all mutant cells, there are genes involved in patterning (*HOX* genes, *MEIS1*) as well as *RND3*, a negative regulator of *RHOA* that is essential for correct neurogenesis[14].

Previously, we identified a group of genes (Supplementary Table 2) that described the different cell populations in the human fetal neocortex and found that cerebral organoids recapitulate the expression pattern of these genes[15]. Using these genes, we reconstructed the lineage relationships between cells and visualized the relationships as intercellular correlation networks for control, *DCHS1* and *FAT4* organoids. As expected, control cells form a network with a topology that recapitulates the layered structure of the healthy developing cortex (Fig. 2d). In contrast, the networks from mutant organoids have a generally deformed architecture, consistent with the observed heterotopia and disorganization of mutant organoids (Fig. 1). Mutant progenitors from *DCHS1* and *FAT4* organoids showed a higher correlation with signatures of the cells located in the inner and outer subventricular zone, at the

Fig. 1 | Mutations in *DCHS1* and *FAT4* cause neuronal heterotopia and disturbances in the morphology of NPCs in cerebral organoids. **a**–**c**,**f**–**f**′′′, Micrographs of sections of organoids immunostained as indicated in the panels. Note the mispositioning of neurons marked by arrows in mutant or in electroporated cerebral organoids. **a**–**c**, batches (b) = 5, organoids (o) = 15 per condition, **f**–**f**′′′, b = 2, o = 6 per condition. **d**,**e**, Classification of organoids according to phenotypes (v = 24 CTRL, 11 *DCHS1*, 16 *FAT4*, v = 23 CTRL2, 17 *DCHS1* KO, 32 *FAT4* KO based on MAP2 staining; v = 7 CTRL, 31 *DCHS1*, 14 *FAT4*, 12 CTRL2, 23 *DCHS1* KO, 17 *FAT4* KO based on NEUN staining). Mutant or KO organoids show significantly more disorganized germinal zones and exclusively show a heterotopia phenotype (chi-squared test, $\chi^2_{(4)} = 84.79$, $P = 0.000$ for **d** in mutant organoids, chi-squared test, $\chi^2_{(4)} = 40.33$, $P = 0.000$ for **d** in KO organoids, chi-squared test, $\chi^2_{(4)} = 27.69$, $P = 0.000$ for **e** in mutant organoids, Chi square test, $\chi^2_{(4)} = 16.94$, $p = 0.000$ for **e** in KO organoids). **b**,**c**, Ectopic nodule of MAP2+ neurons in the germinal zone of *DCHS1* and *FAT4*-mutant organoids. **f**–**f**′′′, Nodule of DCX+ neurons intermingling with NESTIN+ processes of NPCs in the germinal zone after *DCHS1* miRNA electroporation in control organoid. Dotted lines highlight ventricles (V). **g**–**i**, Micrographs of sections of mutant cerebral organoids (day 42) immunostained for NESTIN. Arrows indicate the disrupted morphology of NPCs. **g**–**l**, b = 3, o = 9 per condition. **j**–**l**, Micrographs of sections of mutant organoids electroporated with Gap43-GFP at day 42 and analyzed at day 46. Progenitors in mutant organoids (**k**,**l**) show disrupted pattern (arrows). **m**–**o**, Quantification of the tortuosity index of NPCs based on NESTIN (v = 8 CTRL (c = 43), 4 *DCHS1* (c = 38), 6 *FAT4* (c = 65)) (**m**) or GFP (v = 9 CTRL (c = 44), 5 *DCHS1* (c = 25), 7 *FAT4* (c = 34)) (**n**) staining in mutant organoids, or based on GFP staining in control organoids electroporated with miRNAs against *DCHS1* or *FAT4* (v = 11 CTRL (c = 52), 13 *DCHS1* (c = 71), 7 *FAT4* (c = 49)) (**o**). Results are z scores; significance is based on one-way ANOVA; $P = 0.000$; Holm–Sidak multiple-comparisons test was performed for defining statistical differences between the three genotypes in each graph. Data in graphs are represented as mean ± s.e.m. Scale bars, 100 µm in **a**–**c** and 30 µm in **f**–**f**′′′ and **g**–**l**. Dotted lines highlight ventricles (V). ***$P < 0.001$, ****$P < 0.0001$.

expense of ventricular zone signatures (Fig. 2b,d and Extended Data 3o). This finding supports the observed morphological changes in mutant progenitors, which prematurely delaminate, typical of more-differentiated basally located progenitors (Fig. 1f–o, Extended Data 2l–l‴ and Extended Data 4). Consistent with these findings, more differentiated neurons were found in mutant organoids compared with control organoids in each experiment (Fig. 2b and Extended Data 3p). We further validated these results by analyzing the proportion of proliferating and differentiated cells in patient-derived cerebral organoids by means of FACS analysis (KI67, cycling progenitors; DCX, newborn neurons) from whole organoids (Extended Data 3q–s).

We also aimed at specifically characterizing the migration abilities of neurons with defective *DCHS1* or *FAT4*. To this end, we electroporated control organoids with specific miRNAs targeting *DCHS1* or *FAT4*. 7 d later, we tracked the migratory behavior of the electroporated neurons via time-lapse imaging in 300-µm-thick slices of the organoids with preserved 3D structure (Fig.3a–c). We measured speed of migration (velocity), time neurons spend without moving (resting time points) and ability to move in a straight

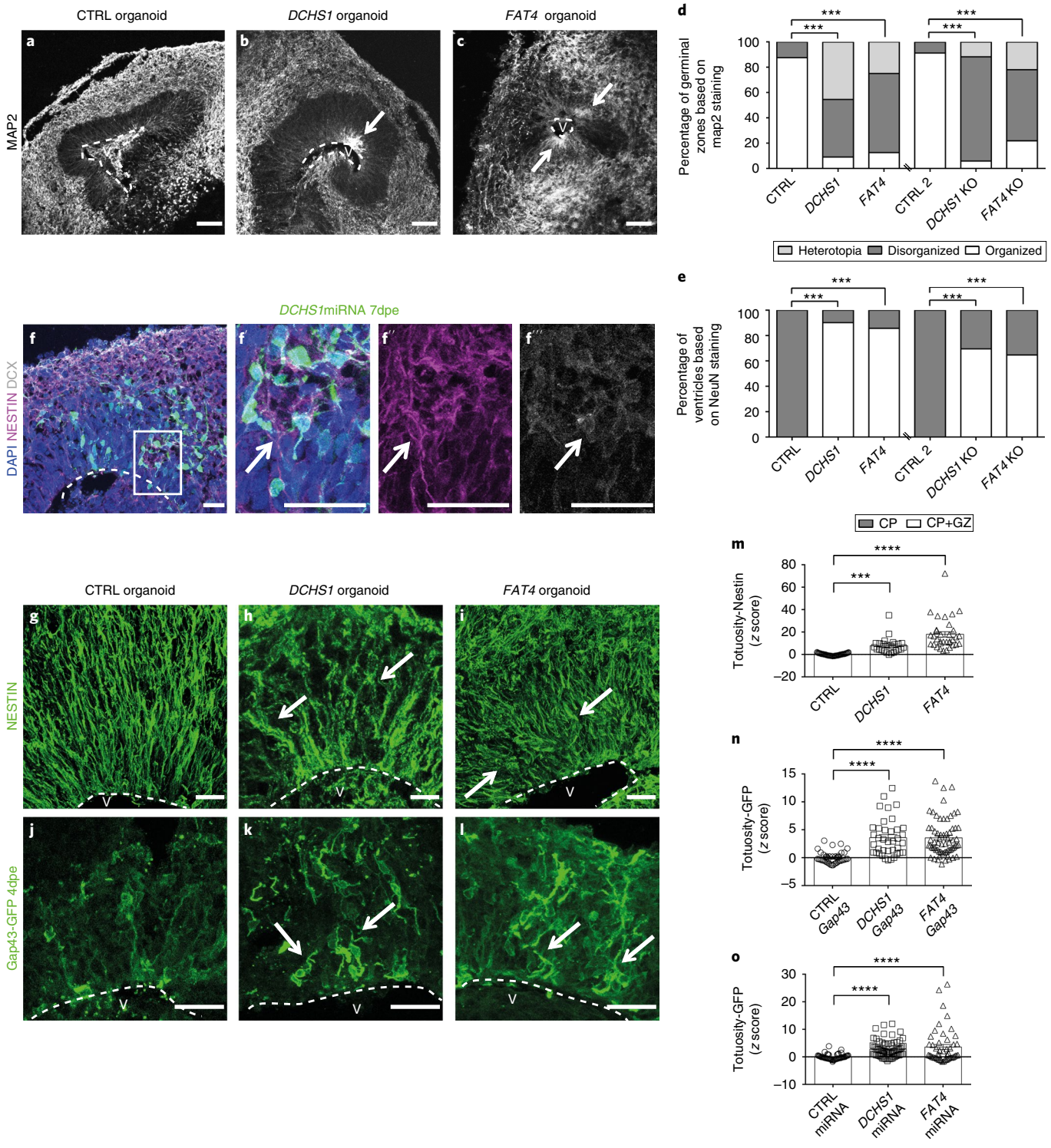

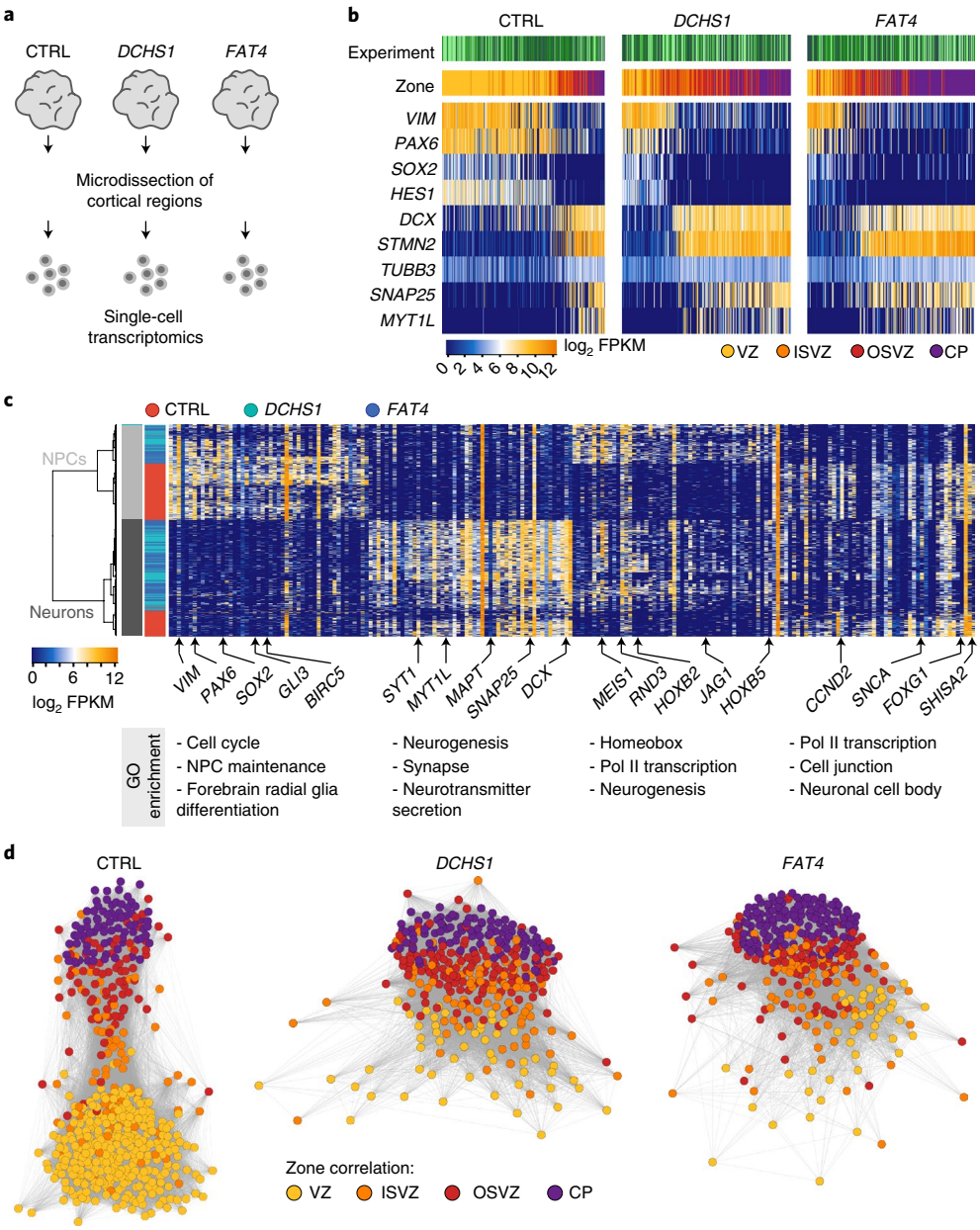

Fig. 2 | scRNA-seq reveals alterations in mutant NPCs. a, Schematic of scRNA-seq experimental procedure. Number of organoids and cells analyzed: 9 organoids (3 for each condition), 805 single cells (316 CTRL, 255 *DCHS1*, 234 *FAT4*). **b**, Heat map showing expression of selected marker genes (rows) for NPCs and neurons for all three conditions (CTRL, *DCHS1*, *FAT4*), with single cells represented in columns. Top side bar visualizes experiment (shades of green) and maximal zone correlation for each single cell (VZ, ventricular zone, yellow; iSVZ, inner subventricular zone, orange; oSVZ, outer SVZ, red; CP, cortical plate, purple). Cells are ordered based on their PC 2 loading, corresponding to the trajectory from NPCs to neurons. **c**, Hierarchical clustering on all 805 single cells (rows) and genes (columns) identified by PCA to correlate and anticorrelate with PC 2 and PC 3 (Supplementary Table 1). The first two components commonly separate progenitors (light gray) from neurons (dark gray) for all experiments. The third component separates CTRL cells (red) from *DCHS1* (cyan) and *FAT4* (blue) cells. Results of gene ontology (GO) enrichment analysis for each gene group are shown below the heat map. **d**, Pairwise correlation network reveals a differentiation topology from NPCs correlating with the VZ (yellow) via cells correlating with iSVZ (orange) and oSVZ (red) to neuronal cells in the CP (purple) for CTRL cells (left), *DCHS1* cells (center) and *FAT4* cells (right).

direction (tortuosity), a typical feature of radially migrating neurons generated in the cerebral cortex. For all three parameters measured, the cells with *DCHS1* or *FAT4* knockdown displayed a significant difference compared with control cells. Specifically, the number of resting time points and the tortuosity were increased, whereas the velocity of the cells decreased (Fig. 3d–f). To investigate if this behavior is an intrinsic feature of the defective neurons or due to the changed NPC scaffold, which we observed in mutant and knockdown *DCHS1* and *FAT4* organoids (Fig. 1 and Extended Data 2,4), we performed time-lapse imaging in cultured mutant cells in a monolayer[16] (Extended Data 6a–f) and tracked the same parameters as those measured in 3D. In accordance with the behavior of migrating neurons observed in 3D, mutant neurons in 2D showed the same significant differences in their migration compared with controls (Fig. 3g–j). To see whether these changes affected only a specific population of cells, we performed hierarchical clustering analysis on the migration behavior of each cell based on all three parameters combined (velocity, resting time

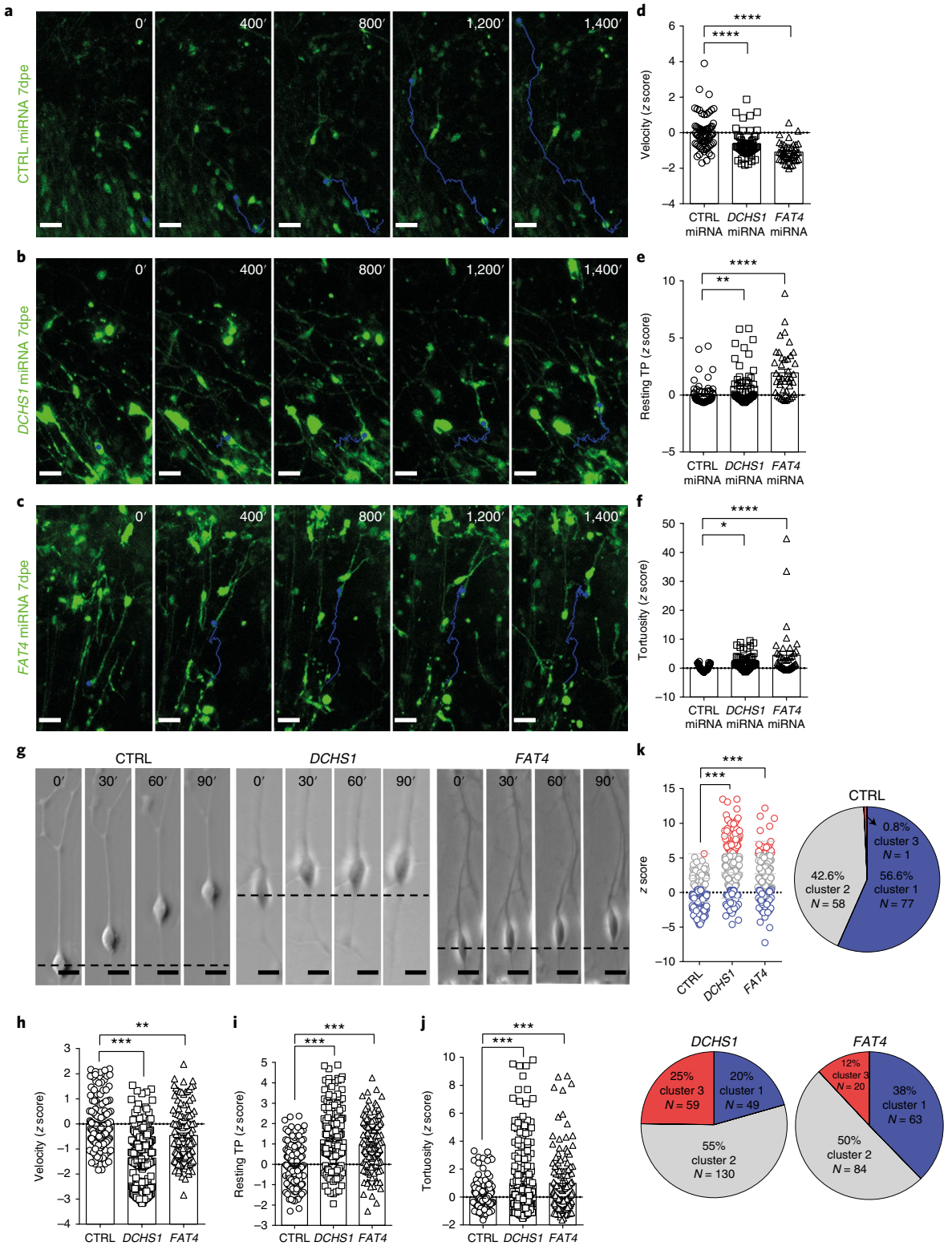

Fig. 3 | Time-lapse imaging of mutant or knockdown neurons reveals an altered migration pattern. a–c,g, Examples of the movement of neuronal somata in control organoids after control, *DCHS1* or *FAT4* miRNA electroporation monitored in 3D time-lapse experiments (**a–c**) and in control and mutant neurons monitored in 2D time-lapse experiments (**g**). Scale bars, 30 µm in **a–c** and 10 µm in **g**. **a–c**, $b=1$, $o=3$ per condition; **g**, $b=4$. **d–f,h–k**, Quantification of velocity, number of resting time points and tortuosity differed according to the mutation. **d–f,h–k**, CTRL miRNA $b=1$, $o=3$, $v=7$, $c=63$; *DCHS1* miRNA $b=1$, $o=3$, $v=7$, $c=56$; *FAT4* miRNA $b=1$, $o=3$, $v=7$, $c=42$; CTRL $b=4$ $c=136$; *DCHS1* $b=4$ $c=220$; *FAT4* $b=4$ $c=126$. Results are *z* scores; statistical analysis was performed in **d**,**e** based on one-way ANOVA, $P=0.000$, Holm–Sidak's multiple comparisons test was performed for defining statistical differences between the three genotypes in each graph, in **h–j** based on one-way ANOVA with Tukey HSD post hoc and through multivariate ANOVA (**h**, $F_{(6,956)}=84.20$, $P=0.000$; **i**, $F_{(6,956)}=43.10$, $P=0.000$, **j**, $F_{(6,956)}=10.68$, $P=0.000$). **k**, Hierarchical and two-step cluster analysis of migration dynamics across the whole cell population (chi-squared test, $\chi^2_{(2)}=70.32$, $P=0.000$). Data in graphs are represented as mean ± s.e.m. $^*P<0.05$, $^{**}P<0.01$, $^{***}P<0.001$, $^{****}P<0.0001$.

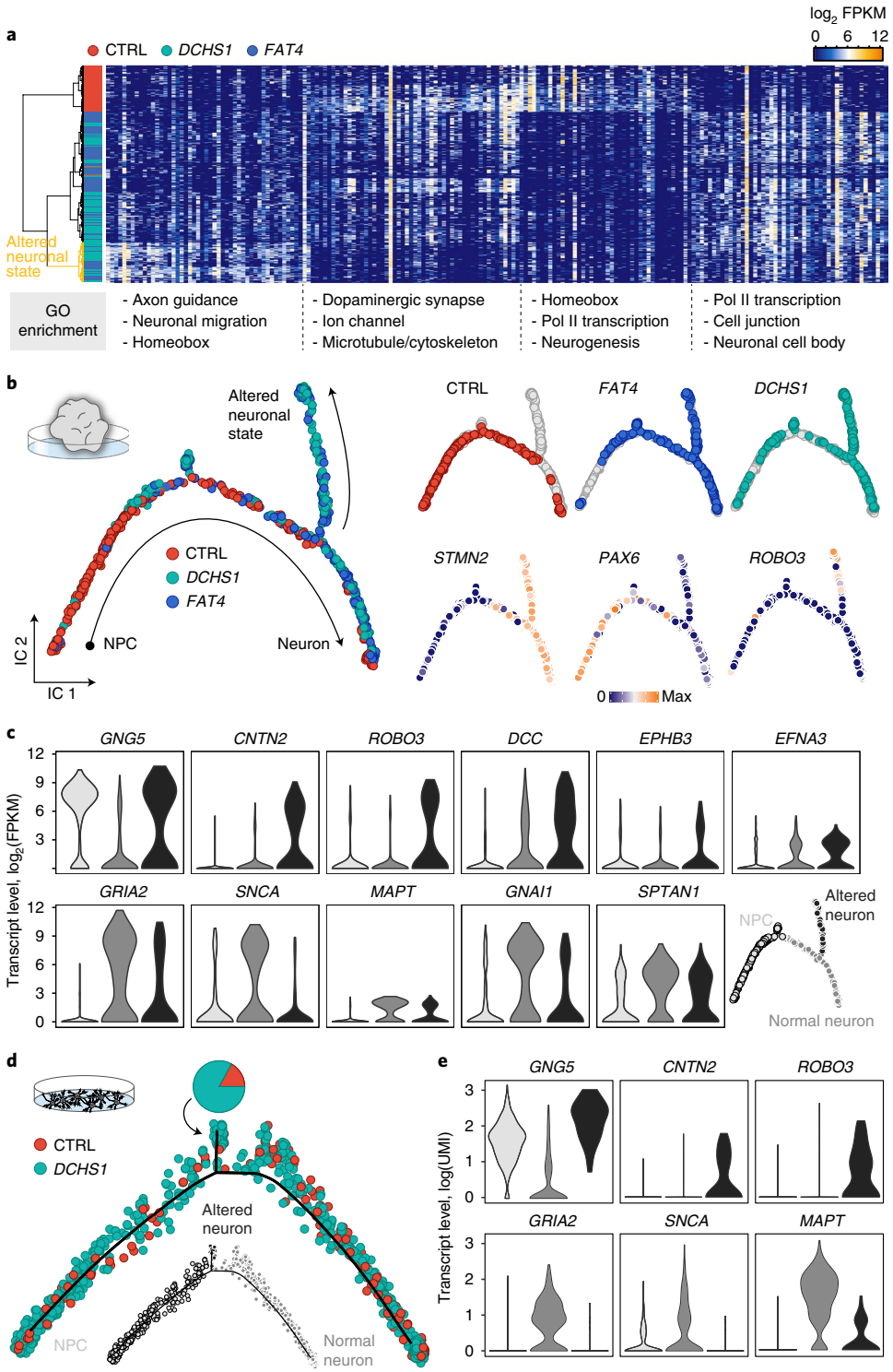

Fig. 4 | scRNA-seq reveals an altered population of neurons. a, Hierarchical clustering on all neurons (rows, 467 single cells) and genes (columns) identified by PCA (Supplementary Table 3). A specific subpopulation of neurons (yellow) is identified that is only found in *DCHS1* or *FAT4* patient-derived organoids. Results of GO enrichment analysis for each gene group are shown below the heat map. **b**, Monocle2 lineage reconstruction of all 805 single organoid cells (circles) using genes identified by PCA (Supplementary Table 3) on all cells and on all neurons reveals a specific subpopulation of neurons only existing in mutant organoids that bifurcates from the general NPC-to-neuron trajectory. The three top right visualizations show cells from each condition separately in their respective color, with all other cells in gray. The three bottom right visualizations show the lineage reconstruction color coded by the expression of three selected genes marking neurons (*STMN2*), NPCs (*PAX6*) and the altered neuronal state (*ROBO3*). **c**, Violin plots show distribution of expression of genes that are up- (top) or downregulated (bottom) in the population of altered (black) compared with normal (dark gray) neurons. NPCs, light gray. Violin plots were plotted using ggplot2 default kernel density settings. **d**, Monocle2 lineage reconstruction of 10X genomics-based scRNA-seq data (437 CTRL, 751 *DCHS1*) from control and *DCHS1*-mutant neuronal cells grown in 2D culture reveals an altered neuronal subpopulation that bifurcates from the general NPC-to-neuron trajectory and is strongly enriched for mutant cells (83% of cells on this branch are *DCHS1* mutant). For the lineage reconstruction, the same genes were used as in **b**. **e**, Violin plots show distribution of expression of genes that are up- (top) or downregulated (bottom) in the population of altered (black) compared to normal (dark gray) neurons. NPCs, light gray. Note that these genes are the same as those found differentially expressed in the organoid altered neuronal state (**c**). IC, independent component.

points and tortuosity). These data revealed that control cells cluster in two main distinct migration behaviors (cluster 1 and cluster 2). Remarkably, in mutant cells, cluster 2 remained the same as that in the control cells, whereas another type of migration behavior, cluster 3, emerged at the expense of cluster 1 (Fig. 3k). This change in the migratory dynamics of a specific cell population of patient-derived neurons could elucidate the phenotype observed in patients where only a limited number of neurons fail to migrate to their final location, resulting in heterotopic neurons residing at the ventricular surface.

We searched for a molecular signature that might explain the altered migration dynamics in a subset of mutant neurons. We used PCA and lineage reconstruction analysis (Monocle2)[17] of the organoid scRNA-seq data and found a subpopulation of neurons in *DCHS1*- and *FAT4*-mutant organoids that was not present in control organoids (Fig. 4a and Supplementary Table 3). This altered neuronal state consisting of mutant cells bifurcates from a progenitor-to-neuron trajectory that includes cells from all three conditions (Fig. 4b). Notably, this lineage bifurcation is not due to the emergence of neuronal cells with a different regional identity in the mutant organoids, because mutant, KO and control organoids express basic neuronal and cortical markers in a similar way (Extended Data 7a–m). The genes upregulated in the altered neuronal population are involved in fundamental neurodevelopmental processes like axon guidance, neuronal migration and patterning (e.g., *ROBO3*, *NDNF*, *DCC*, *CNTN2*, *EPHB3*, *EFNA3*, *ITGB1*, *GNG5*, *HOX*) (Fig. 4c). Interestingly, some genes such as *GNG5* are expressed in progenitors, and are turned off in neurons from control organoids, but stay on in this altered neuronal state. Other genes such as *ROBO3* or *CNTN2* are only found in this subpopulation. On the contrary, the genes downregulated in these cells are involved in synapse formation, ion channel, axon guidance and cytoskeleton (e.g., *GRIA2*, *SNCA*, *MAPT*, *MAP1B*, *GNAI1*, *SPTAN1*, *FLRT2*). Interestingly, three of the dysregulated genes—*MAPT*, *MAP1B* and *SPTAN1*—are associated with epilepsy, a phenotype found in these patients[9,18]. Variants in the *MAP1B* locus have also been associated with PH[9]. To further validate these data, we performed scRNA-seq (10X genomics) on neuronal cells derived from control or *DCHS1*-mutant cells in 2D cultures (Fig. 4d). Consistent with previous results, Monocle2 lineage reconstruction analysis revealed an altered neuronal state enriched for *DCHS1*-mutant cells (83% of altered neuronal cells) compared with control cells (17% of altered neuronal cells), which was characterized by a dysregulation of the same set of genes, as found in the organoid data (Fig. 4c), such as *GNG5*, *CNTN2* and *GRIA2* (Fig. 4e).Taken together, these findings suggest that the subpopulation of the heterotopically located neurons could be the consequence of alterations in migration dynamics due to incorrect regulation of specification and guidance gene programs. Similarly, not all neurons are affected in human patients with PH, but only a subset of them form periventricular clusters. It remains to be explored why the majority of neurons are able to navigate their way up to the cortical plate, despite the fact that they harbor the same gene mutation as the neurons located in the heterotopic clusters.

Molecular and cellular analysis of organoids and cells derived from patients with mutations in *DCHS1* and *FAT4* or upon knockdown of these genes revealed a species-specific role of DCHS1 and FAT4 in human cells. Neuronal heterotopia develops as a consequence of multiple defects: the defective radial progenitor cells, which should guide the neurons to the correct final destination, and a specific subpopulation of neurons that acquire an altered navigation system, which changes their migratory dynamics and leads to compromised equipment for synaptic signaling. It is also clear that in patients, PH is induced by mutations in different genes, and thus it may involve the dysregulation of different molecular pathways[9]. Although the precise molecular regulation of *DCHS1* and *FAT4* remains to be clarified, we propose that changes in the expression of genes involved in the cytoskeleton and cell junction or axon guidance could affect the morphology of progenitor cells and migrating neurons, respectively.

The knowledge of the new molecular signatures acquired from disease neurons could ultimately be used to develop new strategies for targeting neurons that are aberrantly integrated into cortical circuits and possibly cause neuronal heterotopia in patients.

Online content

Any methods, additional references, Nature Research reporting summaries, source data, statements of data availability and associated accession codes are available at https://doi.org/10.1038/s41591-019-0371-0.

Received: 5 January 2018; Accepted: 18 January 2019;
Published online: 11 March 2019

References

1. Cappello, S. et al. Mutations in genes encoding the cadherin receptor-ligand pair DCHS1 and FAT4 disrupt cerebral cortical development. *Nat. Genet.* **45**, 1300–1308 (2013).
2. Romero, D. M., Bahi-Buisson, N. & Francis, F. Genetics and mechanisms leading to human cortical malformations. *Semin. Cell. Dev. Biol.* **76**, 33–75 (2018).
3. Mansour, S. et al. Van Maldergem syndrome: further characterisation and evidence for neuronal migration abnormalities and autosomal recessive inheritance. *Eur. J. Hum. Genet.* **20**, 1024–1031 (2012).
4. Liu, J. S. Molecular genetics of neuronal migration disorders. *Curr. Neurol. Neurosci. Rep.* **11**, 171–178 (2011).
5. Cardoso, C. et al. Periventricular heterotopia, mental retardation, and epilepsy associated with 5q14.3-q15 deletion. *Neurology* **72**, 784–792 (2009).
6. Dubeau, F. et al. Periventricular and subcortical nodular heterotopia. A study of 33 patients. *Brain* **118**(Pt 5), 1273–1287 (1995).
7. Tassi, L. et al. Electroclinical, MRI and neuropathological study of 10 patients with nodular heterotopia, with surgical outcomes. *Brain* **128**, 321–337 (2004).
8. Aghakhani, Y. et al. The role of periventricular nodular heterotopia in epileptogenesis. *Brain* **128**, 641–651 (2005).
9. Heinzen, E. L. et al. De novo and inherited private variants in MAP1B in periventricular nodular heterotopia. *PLoS Genet.* **14**, e1007281 (2018).
10. O'Neill, A. C. et al. A primate-specific isoform of PLEKHG6 regulates neurogenesis and neuronal migration. *Cell Rep.* **25**, 2729–2741.e6 (2018).
11. Lancaster, M. A. & Knoblich, J. A. Generation of cerebral organoids from human pluripotent stem cells. *Nat. Protoc.* **9**, 2329–2340 (2014).
12. Ishiuchi, T., Misaki, K., Yonemura, S., Takeichi, M. & Tanoue, T. Mammalian fat and dachsous cadherins regulate apical membrane organization in the embryonic cerebral cortex. *J. Cell Biol.* **185**, 959–967 (2009).
13. Cappello, S. et al. The Rho-GTPase cdc42 regulates neural progenitor fate at the apical surface. *Nat. Neurosci.* **9**, 1099–1107 (2006).
14. Pacary, E. et al. Proneural transcription factors regulate different steps of cortical neuron migration through Rnd-mediated inhibition of RhoA signaling. *Neuron* **69**, 1069–1084 (2011).
15. Camp, J. G. et al. Human cerebral organoids recapitulate gene expression programs of fetal neocortex development. *Proc. Natl Acad. Sci. USA* **112**, 15672–15677 (2015).
16. Topol, A., Tran, N. N. & Brennand, K. J. A guide to generating and using hiPSC derived NPCs for the study of neurological diseases. *J. Vis. Exp.* https://doi.org/10.3791/52495 (2015).
17. Qiu, X. et al. Reversed graph embedding resolves complex single-cell developmental trajectories.. *Nat. Methods* **14**, 979–982 (2017).
18. Wang, J. et al. Epilepsy-associated genes. *Seizure* **44**, 11–20 (2017).

Acknowledgements

We thank the families participating in this study for their involvement. We thank Y. Lu for help generating the microRNAs, M. Karow and I. Buchsbaum for helping with experiments and fruitful discussions in the lab, T. Öztürk for excellent technical support, A. Weigert for organoid culture, J. Kageyama for helping with data processing, R. Snabel for helping with Smart-seq2 libraries, the Core Unit Flow Cytometry at the Zentrum für Infektionsmedizin (veterinary faculty of the University of Leipzig) and the Core Unit Qualitätsmanagement/Technologieplattform at the Sächsischer Inkubator für Klinische Translation (SIKT) in Leipzig for karyotyping. This work was supported by funding from the DFG CA1205/2-1 (S.C.), ForIPS (M.G.), by the Max Planck Society (S.C., B.T.), by the Boehringer Ingelheim Fonds (S.K.), by the Health Research Council of NZ and Curekids (S.P.R.) and by an ERC Starting Grant (B.T.).

Author contributions

S.C. conceived and designed the research project, J.K., S.K., C.K., A.C.A.-M., R.D.G., S.R., A.C.O., C.T., M. Santel. and E.R. performed experiments and collected data, J.K., C.K., S.K., J.G.C., M. Schroeder, B.T. and S.C. analyzed data, M.D. reprogrammed patients' samples, M.G. was involved in the start of the project, contributed to data discussion and supervision of J.K. S.P.R. was involved in patient sample collection and critical discussion, J.K., S.K., C.K., B.T. and S.C. wrote the manuscript. All authors provided ongoing critical review of results and commented on the manuscript.

Competing interests

The authors declare no competing interests.

Additional information

Extended data is available for this paper at https://doi.org/10.1038/s41591-019-0371-0.

Supplementary information is available for this paper at https://doi.org/10.1038/s41591-019-0371-0.

Reprints and permissions information is available at www.nature.com/reprints.

Correspondence and requests for materials should be addressed to B.T. or S.C.

Methods

Genetic mutation in DCHS1 and FAT4. Details about the genetic mutations found in *DCHS1* and *FAT4* patients can be found in the Supplementary Table 4.

iPSC culture. iPSCs were regularly maintained on Geltrex-coated dishes (Thermo Fisher, Waltham, MA, USA) in mTesR1 medium (Stem Cell Technologies, Vancouver, Canada) at 37 °C, 5% CO_2 and ambient oxygen level. Passaging was done manually by scraping the cells after 10 min of collagenase treatment (Stem Cell Technologies).

Generation of iPSC lines were generated with patient consent, and this study was ethically approved (CEN/11/12/066 Central Regional Ethics Committee, New Zealand and 115–16 Ethical Committee LMU Munich, Germany).

Reprogramming of fibroblasts. 2.5×10^{-5} NuFF3-RQ human newborn foreskin feeder fibroblasts (GSC-3404, GlobalStem) were seeded per well of a 6-well tissue culture dish with advanced MEM (12491015, Thermo Fisher Scientific) supplemented with 5% HyClone FBS (SV30160.03HI, GE Healthcare), 1% MEM NEAA and GlutaMAX (11140050; 35050061 Thermo Fisher Scientific). Patient fibroblasts were obtained from skin biopsies. Day 1, patients and control fibroblast cultures (CTRL-2522, ATCC) of 70–80% confluency were dissociated using 0.25% trypsin-EDTA (25200056, Life Technologies), counted and seeded on the NuFF3-RQ cells at two different densities: 2×10^{-4} cells/well and 4×10^{-4} cells/well. Day 2, medium was changed to Pluriton Reprogramming Medium (00–0070, Stemgent) supplemented with 500 ng/ml carrier-free B18R Recombinant Protein (03–0017, Stemgent). Days 3–18, modified mRNA (mmRNA) cocktail was transfected daily combining *OCT4, SOX2, KLF4, LIN28* and *C-MYC* mmRNAs at a 3:1:1:1:1 stoichiometric ratio and Opti-MEM I Reduced Serum Medium (13778150, Thermo Fisher Scientific) in a total volume of 105 µl with a mix of 92 µl Opti-MEM I Reduced Serum Medium and 13 µl Lipofectamine RNAiMAX Transfection Reagent (31985062, Thermo Fisher Scientific) after incubation at room temperature (RT) for 15 min. Cells were transfected for 4 h, then washed, and fresh reprogramming medium supplemented with B18R was added to the cultures. The mmRNA factors were provided by the RNA CORE of the Houston Methodist Hospital and contained the following modifications: 5-methyl CTP, Pseudo-UTP, ARCA cap and a 150-nucleotide poly-A tail. The first morphological changes were noticed as early as day 5 after the first transfection, and the first iPSC colonies appeared by day 12–15. On day 16, medium was changed to STEMPRO hESC SFM (A1000701, Thermo Fisher Scientific) for 5 d. The iPSC colonies were then harvested using 2 mg/ml collagenase, type IV (17104019, Thermo Fisher Scientific) solution in DMEM/F12 (31331093, Thermo Fisher Scientific) by 40-min incubation at 37 °C. The iPSCs were plated on γ-irradiated mouse embryonic fibroblasts (MEFs) and grown in STEMPRO for ten additional passages before adapting the iPSCs to a feeder-free culture system using plates coated with LDEV-Free Geltrex (A1413302, Thermo Fisher Scientific) and mTeSR1 (05850, StemCell Technologies).

CRISPR genome editing for generation of knockout iPSC lines. 409-B2 human iPSCs with a doxycycline-inducible Cas9 nickase (D10A mutation) were incubated with media containing 2 µg/ml doxycycline (Clontech, 631311) 2 d prior to the addition of gRNA by lipofection or electroporation, as described by Riesenberg and Maricic[19]. Genome editing of *DCHS1* and *FAT4* was done by lipofection and electroporation of gRNA (duplex of chemically synthesized crRNA and tracrRNA, alt-CRISPR IDT), respectively. Lipofection by RNAiMAX (Invitrogen, 13778075) was done using a final concentration of 7.5 nM of each gRNA (DCHS1_target1: GTGGACATCAGCATTGTGCC, DCHS1_target2: GGGCACTGGGTTCTGCCTGT). Electroporation was done using the B-16 program of the Nucleofector 2b Device (Lonza) in cuvettes for 100 µl Human Stem Cell nucleofection buffer (Lonza, VVPH-5022) and 0.3 nmol gRNA (FAT4_target1: TTTGATGCTTTCAAAGAAGG, FAT4_target2: GAGATCCTTCTCCGGCAGAG). Edited cells were plated in different wells for analysis and further propagation. 3 d after addition of gRNA, cells for analysis were dissociated using Accutase (SIGMA, A6964), pelleted, resuspended in 15 µl QuickExtract (Epicentre, QE0905T) and incubated at 65 °C for 10 min, 68 °C for 5 min, and finally 98 °C for 5 min. PCR was done in a T100 Thermal Cycler (Bio-Rad) using the KAPA2G Robust PCR Kit (SIGMA, KK5024) with supplied buffer B and 3 µl of cell extract in a total volume of 25 µl. The thermal cycling profile of the PCR was: 95 °C 3 min; 34× (95° 15 s, 65 °C 15 s, 72 °C 15 s); 72 °C 60 s (DCHS1_forward: GGGTTGTGTGCCTGGACTAT, DCHS1_reverse: TTCCTCTCAGGGCTGTTGAC, FAT4_forward: TAGGGACTGCTGTGCAACTG, FAT4_reverse: AGCTCACAGCCAATCTTCGT) . Sample-specific indices on P5 and P7 Illumina adapters were added in a second PCR reaction using Phusion HF MasterMix (Thermo Scientific, F-531L) and 0.3 µl of the first PCR product. The thermal cycling profile of the second PCR was: 98 °C 30 s; 25× (98° 10 s, 58 °C 10 s, 72 °C 20 s); 72 °C 5 min. The indexed amplicons were purified using Solid Phase Reversible Immobilization (SPRI) beads[20]. Double-indexed libraries were sequenced on a MiSeq (Illumina), giving paired-end sequences of 2 × 150 bp. After base calling using Bustard (Illumina), adapters were trimmed using leeHom[21], and sequences were analyzed using SAMtools[22]. After confirmed bulk editing success, cells were plated in a single-cell dilution that gave rise to single-cell-derived colonies. DNA isolation and further genotyping of these colonies was done as described above.

DCHS1 genotypes:

This is the amplicon sequence of the *DCHS1* wild type:

wild type:

GGGTTGTGTGCCTGGACTATGCCCACACTGGTGCCTGGTGCCACATC-
CTCTGGCACAGAAAAAACATACTGTAGTTGCTCAAATATGGGTGGTGT-
GGGGGTTCCAGGCACAATGCTGATGTCCACTCGGGCACTGGGTTCTGC-
CTGTAGGCCACCTCCGTCCTCAGCCCCGATCTCCAGCTGCACCACAGAAT
TGGCCCGTCTGGCCAAGGGCCAGGCTACTGTCAACAGCCCTGAGAGGAA

3'5' frame 1

F L S G L L T V A W P L A R R A N S V V Q L E I G A E D G G G L Q A E P
S A R V D I S I V P G T P T P P I F E Q L Q Y V F S V P E D V A P G T S V G I V
Q A H N

These are the amplicon sequences of the *DCHS1* KO:

first allele,

GGGTTGTGTGCCTGGACTATGCCCACACTGGTGCCTGGTGCCACATC-
CTCTGGCACAGAAAAAACATACTGTAGTTGCTCAAATATGGGTGGTGT-
GGGGGTTCCAGGCACTGGGTTCTGCCTGTAGGCCACCTCCGTCCTCAG-
CCCCGATCTCCAGCTGCACCACAGAATTGGCCCGTCTGGCCAAGGGCCA
GGCTACTGTCAACAGCCCTGAGAGGAA

3'5' frame 1

F L S G L L T V A W P L A R R A N S V V Q L E I G A E D G G G L Q A E P S
A W N P H T T H I Stop A T T V C F F C A R G C G T R H Q C G H S P G T Q P

second allele,

GGGTTGTGTGCCTGGACTATGCCCACACTGGTGCCTGGTGCCACATC-
CTCTGGCACAGAAAAAACATACTGTAGTTGCTCAAATATGGGTGGTGT-
GGGGGTTCCAGGCACAAACTGGGTTCTGCCTGTAGGCCACCTCCGTCC-
TCAGCCCCGATCTCCAGCTGCACCACAGAATTGGCCCGTCTGGCCAAGG
GCCAGGCTACTGTCAACAGCCCTGAGAGGAA

3'5' frame 1

F L S G L L T V A W P L A R R A N S V V Q L E I G A E D G G G L Q A E P
S L C L E P P H H P Y L S N Y S Met F F L C Q R Met W H Q A P V W A Stop S
R H T T

FAT4 genotypes

FAT4 WT (wild type)

4,314 reads

TAGGGACTGCTGTGCAACTGTACAGTGCATATGAAGAGAAC-
AATAGAACGTTTCTTTTGGCAGCTGTGAAGCGAAATCATAATCA-
GTATGTGAATCCCAGTGGCGTAGCCACCTTCTTTGAAAGCATCA-
AAGAGATCCTTCTCCGGCAGAGTGGAGTAAAGGTGGAATCTGTG
GATCATGACTCCTGTGTGCATGGCCCATGTCAGAATGGAGGGAG-
CTGTCTACGAAGATTGGCTGTGAGCT

5'3' frame 3

G T A V Q L Y S A Y E E N N R T F L L A A V K R N H N Q Y V N P S G V A
T F F E S I K E I L L R Q S G V K V E S V D H D S C V H G P C Q N G G S C L R
R L A V S

FAT4-KO2 (knockout, two different knockout alleles)

6,076 reads

TAGGGACTGCTGTGCAACTGTACAGTGCATATGAAGAGAACAATAGA-
ACGTTTCTTTTGGCAGCTGTGAAGCGAAATCATAATCAGTATGTGAAT-
CCCAGTGGCGTAGCCACCTTCTCCGGCAGAGTGGAGTAAAGGTGGAAT-
CTGTGGATCATGACTCCTGTGTGCATGGCCCATGTCAGAATGGAGGGAG
CTGTCTACGAAGATTGGCTGTGAGCT

5'3' frame 3

G T A V Q L Y S A Y E E N N R T F L L A A V K R N H N Q Y V N P S G V
A T F S G R V E Stop R W N L W I Met T P V C Met A H V R Met E G A V Y E D
W L Stop A

5,345 reads

TAGGGACTGCTGTGCAACTGTACAGTGCATATGAAGAGAACAATAGA-
ACGTTTCTTTTGGCAGCTGTGAAGCGAAATCATAATCAGTATGTGAAT-
CCCAGTGGCGTAGCCACCTTCTTTCCGGCAGAGTGGAGTAAAGGTGGA-
ATCTGTGGATCATGACTCCTGTGTGCATGGCCCATGTCAGAATGGAGGGA
GCTGTCTACGAAGATTGGCTGTGAGCT

5'3' frame 3

G T A V Q L Y S A Y E E N N R T F P P A E W S K G G I C G S Stop L L C A W P Met S E W R E L S T K I G C E

FAT4-KO3 (knockout, two different knockout alleles)

4,878 reads

TAGGGACTGCTGTGCAACTGTACAGTGCATATGAAGAGAACAATAGA-
ACGTTTCTTTTGGCAGCTGTGAAGCGAAATCATAATCAGTATGTGAAT-
CCCAGTGGCGTAGCCACCTTCTCCGGCAGAGTGGAGTAAAGGTGGAAT-
CTGTGGATCATGACTCCTGTGTGCATGGCCCATGTCAGAATGGAGGGAG
CTGTCTACGAAGATTGGCTGTGAGCT

5'3' frame 3

G T A V Q L Y S A Y E E N N R T F L L A A V K R N H N Q Y V N P S G V
A T F S G R V E Stop R W N L W I Met T P V C Met A H V R Met E G A V Y E D
W L Stop A

4,396 reads

TAGGGACTGCTGTGCAACTGTACAGTGCATATGAAGAGAACAATAGA-ACGTTTCTTTTGGCAGCTGTGAAGCGAAATCATAATCAGTATGTGAAT-CCCAGTGGCGTAGCCACCTTCTTTGAAAGCATCAAGGCAGAGTGGAGTA AAGGTGGAATCTGTGGATCATGACTCCTGTGTGCATGGCCCATGTCAGAA TGGAGGGAGCTGTCTACGAAGATTGGCTGTGAGCT

5′3′ frame 3

G T A V Q L Y S A Y E E N N R T F L L A A V K R N H N Q Y V N P S G V A T F F E S I K A E W S K G G I C G S Stop L L C A W P Met S E W R E L S T K I G C E

Generation of microRNA against *DCHS1* and *FAT4*. Three miRNA targeting *FAT4* or *DCHS1*, respectively, were cloned into a pENTR entry vector (BlockIT, Invitrogen, Thermo Fisher) and then recombined into a PCAGGS destination vector according to the manufacturer's protocol (BlockIT, Invitrogen, Thermo Fisher). For validation, vectors were electroporated into SH-SY5Y cells and expression of *FAT4* and *DCHS1* quantified using qPCR.

The sequences of the oligos chosen for experiments are:

DCHS1: TGCTGTACACTGTCAGGTTGATCTCCGTTTTGGCCACTGA CTGACGGAGATCACTGACAG

FAT4: GCTGATCAGTTGCAGTAACAGAGGAGTTTTGGCCACTGACT GACTCCTCTGTCTGCAACT

The qPCR primers sequences used for validation are:

DCHS1-fw: 5′TGCACCTGAAGACACGGTAT 3′

DCHS1-rev: 5′CAGAGGCCTCATAAGCCGTA 3′

FAT4-fw: 5′CTTCCAAATGGACCCTGAGA 3′

FAT4-rev: 5′CGGTGCCCACTTGAGCATTC 3′

Generation of NPCs and neurons. Neural progenitors were generated as described previously[23] with modifications. In short, embryoid bodies were generated from iPSCs by plating colonies in suspension in neural induction medium consisting of DMEM F12 with N2 and B27 supplements (Thermo Fisher). Embryoid bodies were plated on polyornithine and laminin (Sigma Aldrich, St. Louis, MO, USA) coated dishes and cultured for 7 d in neural induction medium. Neural rosettes were manually picked using a stereological microscope (Nikon, Tokyo, Japan) and a P1000 tip, manually dissociated and further cultivated in neural progenitor medium (neural induction medium supplemented with bFGF at 20 ng/ml, Peprotech, Rocky Hill, NJ, USA). For passaging, the cells were dissociated using Accutase (Stem Cell Technologies) and split at a maximum ratio of 1:3.

Generation and analysis of cerebral organoids. Cerebral organoids were generated as previously described[24]. Organoids were kept in 10-cm dishes on an orbital shaker at 37 °C, 5% CO_2 and ambient oxygen level with medium changes every 3 to 4 d. Organoids were analyzed at 20 d, 42 d and 70 d after plating. For immunostaining, 16-µm sections of organoids were prepared using a cryotome. At least five different organoids for each of three different batches were analyzed.

Electroporation of organoids. For electroporation, organoids were kept in neural differentiation medium as described[11] without antibiotics. The organoids were placed in an electroporation chamber (Harvard Apparatus, Holliston, MA, USA), and plasmid DNA was injected at a concentration of 1 µg/µl at several positions. The organoids were then subjected to five pulses at 80 V with a 50-ms duration in an interval of 500 ms using an ECM830 electroporation device (Harvard Apparatus).

3D time-lapse imaging. For 3D time-lapse imaging, slices of electroporated cerebral organoids were prepared and imaged as described previously[25]. Briefly, organoids were sliced at 300-µm thickness on a vibratome (Leica VT1200S) in ice-cold DMEM/F12 (Invitrogen) supplement with sodium bicarbonate, glucose and 10% antibiotics, oxygenated with 100% O_2 for 20 min before cutting. The slices were placed on a cell culture insert (Millicell) and further cultured in normal organoid medium. The slices were kept in an atmosphere with 5% CO_2 at 37 °C. Live imaging was performed for 48 h using Leica TCS SP8 Confocal microscope (Leica, Germany), taking an image every twenty minutes. The cell movement was tracked using ImageJ software and the Manual Tracking Plugin, and the movement parameters calculated and analyzed in GraphPad Prism.

2D time-lapse imaging. For 2D time-lapse imaging, cultures of neural progenitor cells were kept in neural progenitor medium without bFGF for 7 d to allow cells to differentiate. Consequently, live imaging was performed for 3 d using Zeiss Axiovision Observer Fluorescent Microscope (Zeiss, Germany) and Zen Software, taking an image every 5 min. The cell movement was tracked using ImageJ software and the Manual Tracking Plugin, and the movement parameters calculated and analyzed using R. Neuronal identity was confirmed using TUBB3 immunostaining at the end of the imaging experiment.

Dissociation of organoids and neuronal cells in 2D culture for scRNA-seq. Organoids were microdissected to enrich for cortical tissue and washed twice with 2 ml of HBSS ($-Ca^{2+}/-Mg^{2+}$ (w/o), Sigma). The tissue was dissociated using a papain-based neural tissue dissociation kit (Miltenyi) with multiple intermittent triturations using wide-bore pipette tips and p1,000 and p200 pipettes. After dissociation, cells were filtered through a 30-µm strainer and a 20-µm strainer, washed with HBSS ($+Ca^{2+}/+Mg^{2+}$ (w), Sigma) and spun down at 300*g* for 10 min. Cells were then washed again with HBSS (w), spun down for 5 min at 300*g* and were resuspended in HBSS (w). Counting and viability assessment were performed using Trypan blue staining (Countess automatic cell counter, Invitrogen) for further FACS-based single-cell transcriptomics.

2D differentiated neurons from *DCHS1*, *FAT4* and two controls were detached from wells of a 24-well plate on day 14 after initiation of differentiation into neurons. First, cells were washed with PBS (w/o, Gibco) twice and incubated with 0.5 mM EDTA (Invitrogen) in DPBS (Gibco) + 1% Accutase (v/v, Sigma) for 5 min at 37 °C to detach cells. After incubation, HBSS (w/o, Sigma) was added to the wells, and cells were washed off by rinsing with a 1,000p. Detached cells were spun down 5 min at 300*g* and washed with HBSS (w/o), spun down again and resuspended in HBSS (w/o) for counting.

RNA-seq experiments. Organoids were microdissected to enrich for cortical regions, and the tissue was dissociated using a papain-based neural tissue dissociation kit (Miltenyi). Neuronal cells in 2D culture were brought into single-cell suspension using 1% (v/v) Accutase (Sigma) in DPBS/EDTA (0.5 mM, Gibco, Invitrogen). Single-cell transcriptomic analysis was performed using either the Smart-seq2 protocol[26] (for all organoid experiments), or the 10X genomics chromium platform (for neuronal cells in 2D differentiation). Libraries were prepared using the Illumina Nextera XT DNA Sample Preparation kit (SS2) or according to the 10X genomics Single Cell 3′v2 protocol. Quantification and quality control of the resulting cDNA was performed using high-throughput capillary gel electrophoresis (Fragment analyzer, Advanced Analytical; for SS2) or the Bioanalyzer High Sensitivity DNA Assay (Agilent; for 10X cDNA, for SS2 and 10X libraries). Single-cell cDNA libraries were sequenced on an Illumina HiSeq2500 platform. Reads were processed and aligned to the genome (hg38 sourced from Ensembl or 10X genomics) using TopHat[27] or using the 10X Genomics Cell Ranger software (v 2.1.0), respectively. Data analysis was performed using custom-written R scripts and using the following packages in R: Seurat (v 2.3.0), Monocle2 (v2.0.0 for SS2 data, v 2.6.3 for 10X data), igraph, ggplot2 and FactoMineR.

For Smart-seq2-based scRNA-seq (organoid scRNA-seq dataset), single cells were isolated by FACS of individual cells into individual wells of 96-well plates. cDNA was prepared from each single cell using the previously described Smart-seq2 protocol[26]. Size distribution and concentration of single-cell cDNA was assessed by high-throughput capillary gel electrophoresis (Fragment analyzer, Advanced Analytical). Sequencing libraries were constructed in 96-well plates using the Illumina Nextera XT DNA Sample Preparation kit as described previously[28]. Libraries were quantified by Agilent Bioanalyzer using the High Sensitivity DNA analysis kit. Up to 192 single-cell libraries were pooled and each cell was sequenced 100-bp paired-end on Illumina HiSeq2500. Base calling, adaptor trimming, and demultiplexing was performed as described in refs. [29,30]. For 10X Genomics Chromium based scRNA-seq (2D neuronal differentiation dataset), the 10X Chromium Single Cell 3' Kit v2 was used. Control and mutant cells were mixed for multiplexing (*FAT4*/ CTRL and *DCHS1*/ CTRL) and were loaded on one lane of a 10X microfluidic chip. cDNA cleanup, amplification and library preparation were performed by following the Single Cell 3′ protocol. Quantification and quality control of the resulting libraries was performed using Bioanalyzer (Agilent) High Sensitivity DNA Assay. The resulting two libraries were pooled at equal ratios and sequenced on two lanes of an Illumina HiSeq2500 platform.

Processing, analysis, and graphic display of Smart-seq2-based scRNA-seq data. Raw reads were processed using a custom script and aligned to a Bowtie2 (ref. [31]) indexed human genome (hg38 sourced from Ensembl) using TopHat[27] with default settings. Transcript levels were quantified as Fragments Per Kilobase of Mapped reads (FPKM) generated by Cufflinks[32] using gencode protein coding genes (hg38 Havana). We excluded cells that had less than 100,000 reads or expressed less than 1,000 genes. Transcript levels were converted to the log-space by taking the $\log_2$ (FPKM). R studio (https://www.rstudio.com/) was used to run custom R scripts to perform principal component analysis (PCA, FactoMineR package), hierarchical clustering (stats package), covariance analysis and to construct heat maps, violin plots, scatter plots and dendrograms. Generally, ggplot2 and gplots packages were used to generate data graphs. The Monocle2 package[17] (https://bioconductor.org/packages/release/bioc/html/monocle.html) was employed to analyze cell lineage relationships using 289 genes (Supplementary Table 3) identified via PCA on all cells and on all neurons. Covariance network analysis and visualizations were done using igraph implemented in R (http://igraph.sf.net). Gene ontology enrichment analyses were performed using DAVID informatics Resources 6.7 (ref. [33]). To assign a cortical zone (VZ, iSVZ, oSVZ, CP) to each individual cell, we calculated for each single cell the Spearman correlation of its transcriptome (all genes) with bulk transcriptome data from each of four microdissected cortical zones (VZ, iSVZ, oSVZ, CP, mean expression value of each gene across 4 replicates)[34] as described previously[15]. Generally, we performed PCA on variable genes (variance > 0.5) expressed (> 1 FPKM) in more than two cells. For Figs. 2c and 4a, we extracted the

genes positively and negatively correlating with PC2 and 3, using an absolute PC loading threshold >0.2 with a maximum of 50 genes per PC to avoid individual PCs swamping the analysis, resulting in 200 genes (Supplementary Tables 1 and 3). These genes were plotted in the heat map. The heat map in Extended Data 3o presents the top 50 genes positively and negatively correlating with PC 1. To construct the intercellular correlation networks in Fig. 2d, we computed a pairwise correlation matrix for all cells and using genes discovered in the PCA analysis on cells from the primary human fetal cortex at gestational week 12 and 13 (Supplementary Table 2) as described[15]. We then generated a weighted adjacency network graph using the graph.adjacency() command in igraph and visualized cells as vertices connected to other cells via edges if the Pearson pairwise correlation between two cells was higher than 0.4. The Fruchterman–Reingold layout was used to plot the network graph.

Processing, analysis, and graphic display of 10X genomics–based scRNA-seq data. For the 10X genomics data, base calling, alignment to the human reference GRCh38 (as provided by 10X) and identification of valid cell barcodes was performed using 10X Genomics Cell Ranger software (v 2.1.0). Genotypes for demultiplexing the pooled cell lines in each library were called from merged scRNA-seq organoid datasets of the respective cell lines (*DCHS1*, *FAT4*, CTRL) using bcftools (v 1.4) mpileup and bfctools call. Genotypes for the respective combinations of pooled cell lines were merged using bcftools merge. Demuxlet[35] was used to assign single cells to their respective cell line, taking only valid barcodes into account as defined by Cell Ranger. Cells with insufficient likelihood difference or ALPHA value >0.3 were considered as doublets, and all remaining cells were assigned with their first best cell line assignment as provided by demuxlet. After demultiplexing, most of the cells in the *FAT4*/ CTRL dataset were assigned as CTRL cells, whereas most of the cells in the *DCHS1*/ CTRL dataset were assigned as *DCHS1* cells, which was consistent with the number of cells per line in the cell suspensions loaded on the 10X microfluidic chip device. Thus, we focused the analysis on comparing sufficient numbers of cells of *DCHS1* and CTRL.

Single-cell data were analyzed using the Seurat (v 2.3.0) toolkit for prefiltering and clustering of data. Cells with less than 500 and more than 6,000 genes per cell and more than 10% mitochondrial genes expressed were filtered from the dataset. The normalized data were scaled, and the effect of mitochondrial gene expression and number of UMI's were regressed out. Identification of clusters and t-Stochastic Neighbor Embedding (tSNE) clustering was performed using the first ten principal components based on the highly variable genes in the dataset. Mesenchymal-like cells as revealed by clustering and high expression of DCN and COL1A2 and cells with high cycling gene expression (MKI67 and TOP2A > 1.5 UMI after normalizing) were filtered from the data. Cells were ordered along a pseudotemporal trajectory using Monocle (v 2.6.3) by using DDRTree for dimension reduction and using the same ordering genes that were applied to construct differentiation trajectories for organoids.

Immunohistochemistry. Immunostainings were performed as described previously[1]. Nuclei were visualized using 0.1 µg/ml DAPI (Sigma Aldrich). Immunostained sections were analyzed using Olympus or Leica laser-scanning microscopes. F-ACTIN was visualized by incubation with Alexa Fluor 488–conjugated PHALLOIDIN (Thermo Fisher) according to the manufacturer's protocol. Antibodies list is included in the Supplementary Table 5.

FACS analysis. Cerebral organoids (55–60 d in culture) were collected for FACS analysis. Three to six samples were analyzed; every sample contained two individual organoids. Organoids were enzymatically dissociated with Accutase at 37 °C for 30 min. During incubation, every 10 min, the organoids were triturated with a P1000 pipette. After dissociation, samples were washed in PBS via centrifugation at 1,200 r.p.m. for 5 min. The cell suspension was filtered through a 100-µm cell strainer and centrifuged at 1,200 r.p.m. for 5 min, and the cells were fixed in 70% ice-cold ethanol. After 1 h at –20 °C, samples were centrifuged for 30 min at 2,000 r.p.m. and then resuspended in 5 ml staining solution (PBS containing 1% FCS). After further centrifugation for 30 min at 2,000 r.p.m., the cell pellet was resuspended in staining solution containing anti KI67 antibody (1:200, see antibody's table), or anti DCX antibody (1:1,000, see Supplementary Table 5) and incubated for 30 minutes. After washing in staining solution, cells were resuspended in staining solution containing AlexaFluor546 anti–guinea pig, for DCX, or anti-mouse (1:800), for KI67, secondary antibodies and incubated for 30 min. After washing in PBS, cells were resuspended in PBS. FACS analysis was performed on a FACS Aria (BD) in BD FACS Flow TM medium, with a nozzle diameter of 100 µm. Debris and aggregated cells were gated out by forward scatter and sideward scatter; single cells were gated out by FSC-W/FSC-A. Gating for fluorophores was done using samples stained with secondary antibody only. Flow rate was below 500 events/s.

Western blot. Cells were lysed in lysis buffer (62.5 mM Tris-HCl, pH 6.8, 2% SDS, 10% saccharose in H_2O) with protease and phosphatase inhibitors (Roche, Basel, Switzerland), and 20 µg of protein was separated by SDS-PAGE with a 12% gel. Proteins were transferred to a nitrocellulose membrane (GE Healthcare, Chalfont St Giles, Buckinghamshire, Great Britain). For detection, membranes were incubated with primary antibodies overnight, then with horseradish peroxidase-labeled secondary antibodies at room temperature, and then treated with ECL Western Blotting Detection solution (Millipore, Billerica, MA, USA) to visualize bands. Bands were quantified using ImageJ software.

In situ hybridization. Probes for in situ hybridization were generated as described in ref. [5]. Linearized in situ plasmids were in vitro transcribed using DIG NTP labeling mix, RNA polymerase T7 and Sp6 as well as RNase inhibitor (Roche). In situ mRNA transcript detection was performed according to standard procedures.

Cell and tissue quantifications. For quantification of proliferating apical NPCs, all apically located PH3-positive cells were quantified. Cell counts were normalized by the length of the apical surface. MAP2 and ARL13B fluorescence intensity was quantified using ImageJ software. MAP2 signal was quantified only where progenitors are enriched (ventricular zone). ARL13B signal was quantified at the apical surface and at basal positions. In particular, the ARL13B+ fluorescent signal intensity from all the cilia facing the ventricular lumen versus the rest of the cilia found in the germinal and cortical zones was measured using ImageJ software and normalized per area. The analysis of disorganization of the ventricles in mutant and KO lines was done based on the MAP2 staining. More precisely as heterotopic were called the ventricles, which have clusters of MAP2-positive cells in the germinal zones, and as disorganized were defined the ventricles in which the boundaries between the cortical and germinal zone was not clearly distinguished. The percentage of ventricles with $NEUN^+$ cells only in the cortical plate or having more than five $NEUN^+$ cells the germinal zone in addition to the normal NEUN layer in the cortical plate was quantified. The apical surface was identified using β-CATENIN and PALS1 immunostaining, and the apical distance was measured from the apical surface, defined by the immunostainings, to the cell nuclei, defined by the DAPI, in at least five positions per germinal zone using ImageJ software. The organoid size was measured based on the surface of the organoids using ImageJ software. The thickness of the ventricular zone and cortical plate were manually outlined and measured using ImageJ software. NPCs radial morphology and tortuosity were assessed via manual outlining of the $NESTIN^+$ processes or the GFP^+ processes after electroporation using ImageJ software. The tortuosity index was calculated by dividing the total (segmented) length of the $NESTIN^+$ of GFP^+ processes divided by the straight line connecting the beginning and end of the segmented line. The identity of cells tracked through time lapse in 2D culture was assessed by the expression of MAP2 and DCX.

More details regarding statistical tests applied and individual experiments replicates are found in the figure legends, where b refers to batches, o refers to organoids, v refers to ventricles and c refers to cells.

All analysis was done using the R statistical software package, the GraphPad software and SPSS 20.0.

Reporting Summary. Further information on research design is available in the Nature Research Reporting Summary linked to this article.

Data availability

The scRNA-seq data used in this study have been deposited in the Gene Expression Omnibus under accession number GSE124031. All relevant accession codes are provided. Further details on the methods can be found in the Life Sciences Reporting Summary. Additional data that support the findings of this study are available from the corresponding author upon reasonable request.

References

19. Riesenberg, S. & Maricic, T. Targeting repair pathways with small molecules increases precise genome editing in pluripotent stem cells. *Nat. Commun.* **9**, 2164 (2018).
20. Meyer, M. & Kircher, M. Illumina sequencing library preparation for highly multiplexed target capture and sequencing. *Cold Spring Harb. Protoc.* **2010**, pdb.prot5448 (2010).
21. Renaud, G., Stenzel, U. & Kelso, J. leeHom: adaptor trimming and merging for Illumina sequencing reads. *Nucleic Acids Res.* **42**, e141 (2014).
22. Li, H. et al. The Sequence Alignment/Map format and SAMtools. *Bioinformatics* **25**, 2078–2079 (2009).
23. Boyer, L. F., Campbell, B., Larkin, S., Mu, Y. & Gage, F. H. Dopaminergic differentiation of human pluripotent cells. *Curr. Protoc. Stem Cell Biol.* **Chapter 1**, Unit1H.6 (2012).
24. Lancaster, M. A. et al. Cerebral organoids model human brain development and microcephaly. *Nature* **501**, 373–379 (2013).
25. Pilz, G.-A. et al. Amplification of progenitors in the mammalian telencephalon includes a new radial glial cell type. *Nat. Commun.* **4**, 2125 (2013).
26. Picelli, S. et al. Smart-seq2 for sensitive full-length transcriptome profiling in single cells. *Nat. Methods* **10**, 1096–1098 (2013).

27. Trapnell, C., Pachter, L. & Salzberg, S. L. TopHat: discovering splice junctions with RNA-Seq. *Bioinformatics* **25**, 1105–1111 (2009).
28. Treutlein, B. et al. Reconstructing lineage hierarchies of the distal lung epithelium using single-cell RNA-seq. *Nature* **509**, 371–375 (2014).
29. Renaud, G., Kircher, M., Stenzel, U. & Kelso, J. freeIbis: an efficient basecaller with calibrated quality scores for Illumina sequencers. *Bioinformatics* **29**, 1208–1209 (2013).
30. Renaud, G., Stenzel, U., Maricic, T., Wiebe, V. & Kelso, J. deML: robust demultiplexing of Illumina sequences using a likelihood-based approach. *Bioinformatics* **31**, 770–772 (2015).
31. Langmead, B. & Salzberg, S. L. Fast gapped-read alignment with Bowtie 2. *Nat. Methods* **9**, 357–359 (2012).
32. Trapnell, C. et al. Transcript assembly and quantification by RNA-Seq reveals unannotated transcripts and isoform switching during cell differentiation. *Nat. Biotechnol.* **28**, 511–515 (2010).
33. Huang, D. W., Sherman, B. T. & Lempicki, R. A. Systematic and integrative analysis of large gene lists using DAVID bioinformatics resources. *Nat. Protoc.* **4**, 44–57 (2008).
34. Fietz, S. A. et al. Transcriptomes of germinal zones of human and mouse fetal neocortex suggest a role of extracellular matrix in progenitor self-renewal. *Proc. Natl Acad. Sci.* **109**, 11836–11841 (2012).
35. Kang, H. M. et al. Multiplexed droplet single-cell RNA-sequencing using natural genetic variation. *Nat. Biotechnol.* **36**, 89–94 (2018).

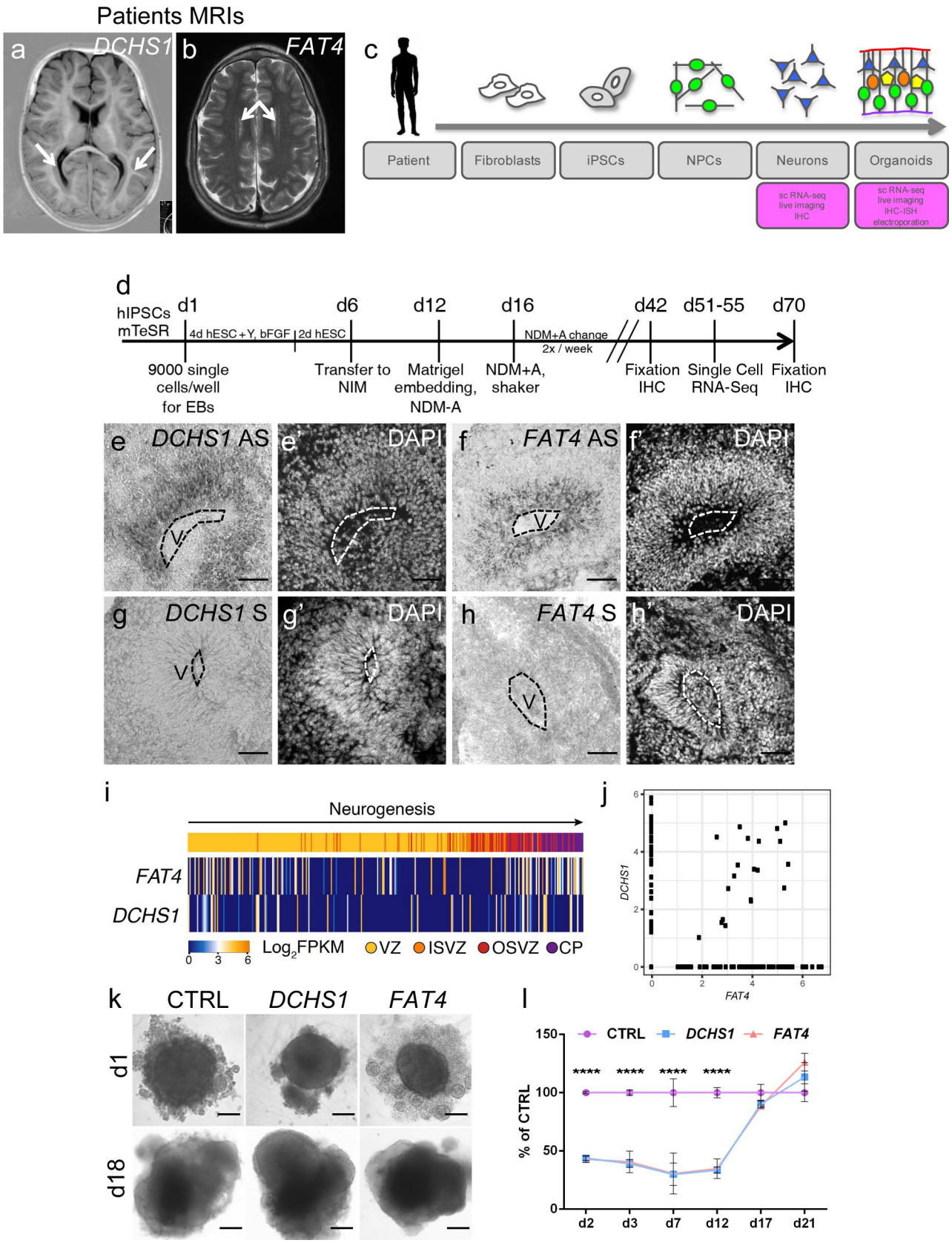

Extended Data Fig.1 | See next page for figure caption.

Extended Data Fig. 1 | Expression of *DCHS1* and *FAT4* in cerebral organoids and temporal development of *DCHS1*- and *FAT4*-mutant organoids. **a**, Axial T1 image demonstrating laminar PH lining the occipital horns and peritrigonal region of the ventricles (arrows). **b**, Axial T2 demonstrating linear lesions iso-intense with cortical gray matter adjacent to the lateral walls of the bodies of the lateral ventricles[2]. **c**, Schematic representation of the main experimental approach used. **d**, Timeline of the organoid generation. EBs, embryoid bodies; hESC, low-bFGF human embryonic stem cell medium; NIM, neural induction medium; Y, Rock inhibitor; NDM, neural differentiation medium; +/− A: B27 supplement with or without vitamin; IHC, immunohistochemistry; RNA-seq, RNA sequencing. **e**–**h**′, Detection of *DCHS1* and *FAT4* by in situ hybridization, $b = 2$, $o = 5$ per condition. **i**,**j**, mRNA expression of *DCHS1* and *FAT4* in single cells ($c = 316$) derived from control organoids, showing similar expression patterns between *DCHS1* and *FAT4* but often in different cells. **i**, Cells (columns) are ordered based on their PC 2 loading, corresponding to the trajectory from NPCs to neurons. Side bar shows maximal zone correlation for each single cell (ventricular zone, VZ, yellow; inner subventricular zone, iSVZ, orange; outer SVZ, oSVZ, red; cortical plate, CP, purple). **j**, Biplot showing transcript levels (in $\log_2$(FPKM)) of *FAT4* (*x* axis) and *DCHS1* (*y* axis) in 316 single cells of control organoids. **k**,**l**, Temporal development of patient-derived cerebral organoids compared with control organoids ($o = 14$ CTRL, 17 *DCHS1*, 17 *FAT4*); the diameters of organoids derived from *DCHS1*- and *FAT4*-mutant cells are slightly smaller compared to those of control organoids until day 12 (d12), shown in **k**. Significance based on two-way ANOVA, $P = 0.000$, Tukey HSD post hoc for multiple comparisons was performed for defining statistical differences between the three genotypes. Dotted lines highlight ventricles (V). Data in graphs are represented as mean ± s.e.m. Scale bars, 100 µm in **e**–**h**′,**k**.

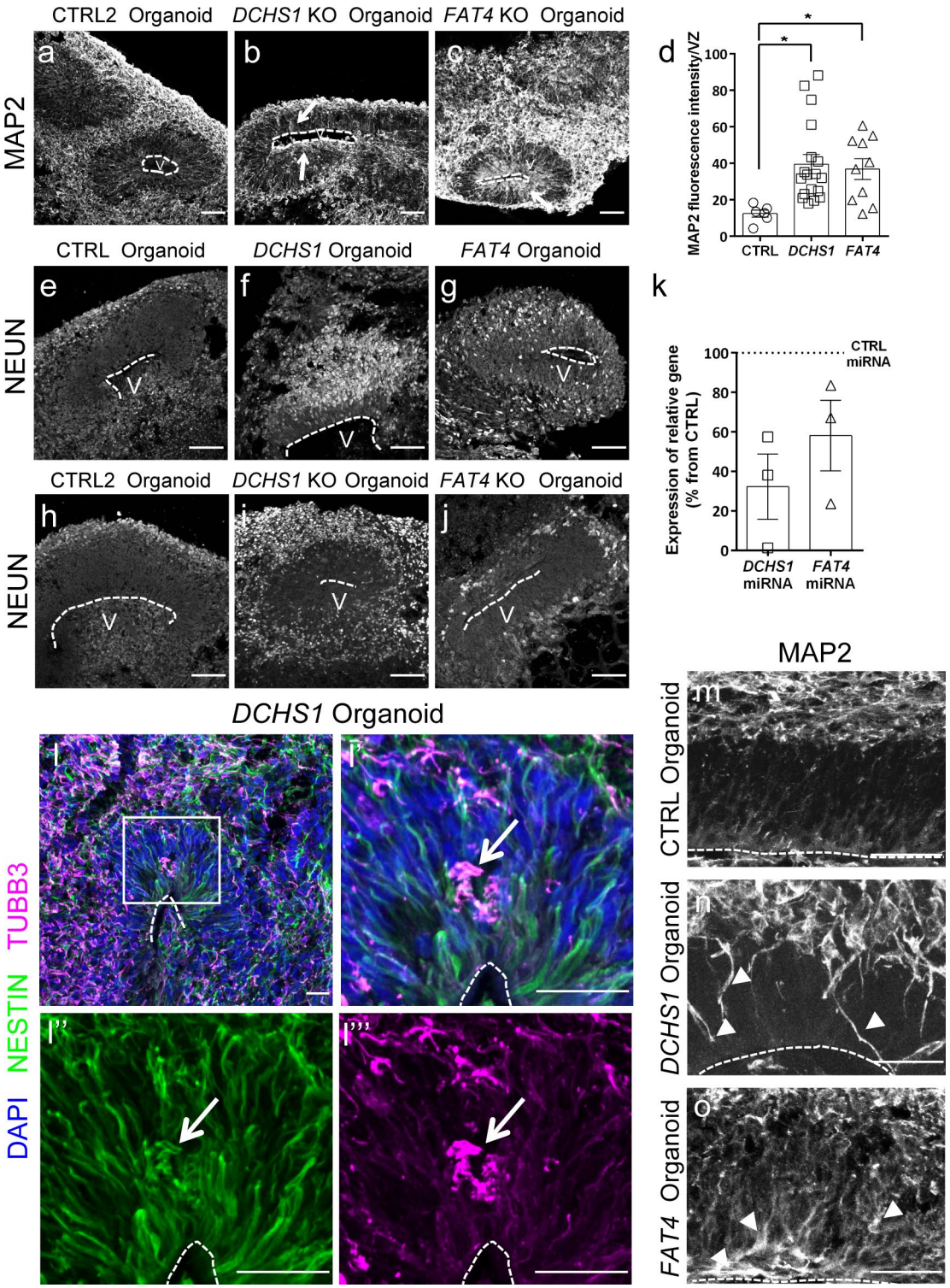

Extended Data Fig. 2 | Heterotopically located neurons in *DCHS1* and *FAT4*-mutant and KO organoids. a–c,e–j,l–o, Micrographs of sections of mutant or KO organoids immunostained as indicated in the panels. Note the mispositioning of neurons marked by arrows in mutant or in electroporated cerebral organoids. **a–c**, $b=2$, $o=6$ per condition; **e–j**, $b=2$, $o=6$ per condition; **l–l'''**, $b=5$, $o=15$ per condition; **m–o**, $b=5$, $o=15$ per condition. **d**, MAP2 fluorescence intensity measured only in the ventricular zones (VZ) ($v=6$ CTRL, 18 *DCHS1*, 11 *FAT4*; significance based on one-way ANOVA, $P=0.0166$, Tukey HSD post hoc for multiple comparisons for defining statistical differences between the three genotypes). **k**, Quantification measured by qPCR of the knockdown of *DCHS1* and *FAT4* by microRNAs (miRNA) against *DCHS1* or *FAT4*, respectively ($b=2$, independent cultures per time = 3 CTRL, 3 miRNA *DCHS1*, 3 miRNA *FAT4*, significance based on one-way ANOVA, $P=0.0377$, Tukey HSD post hoc for multiple comparisons for defining statistical differences between the three genotypes) in SH-SY5Y cells 48 h after nucleofection. **l–l'''**, Nodule of TUBB3+ neurons intermingling with NESTIN+ processes of NPCs in the germinal zone of *DCHS1*-mutant organoids. **m–o** *DCHS1*- and *FAT4*-mutant organoids show changes in the morphology and thickness of their neuritis, as depicted by arrowheads. Dotted lines highlight ventricles (V). Data in graphs are represented as mean ± s.e.m. Scale bars, 100 μm in **a–c** and **e–j** and 30 μm in **l–o** . Source data.

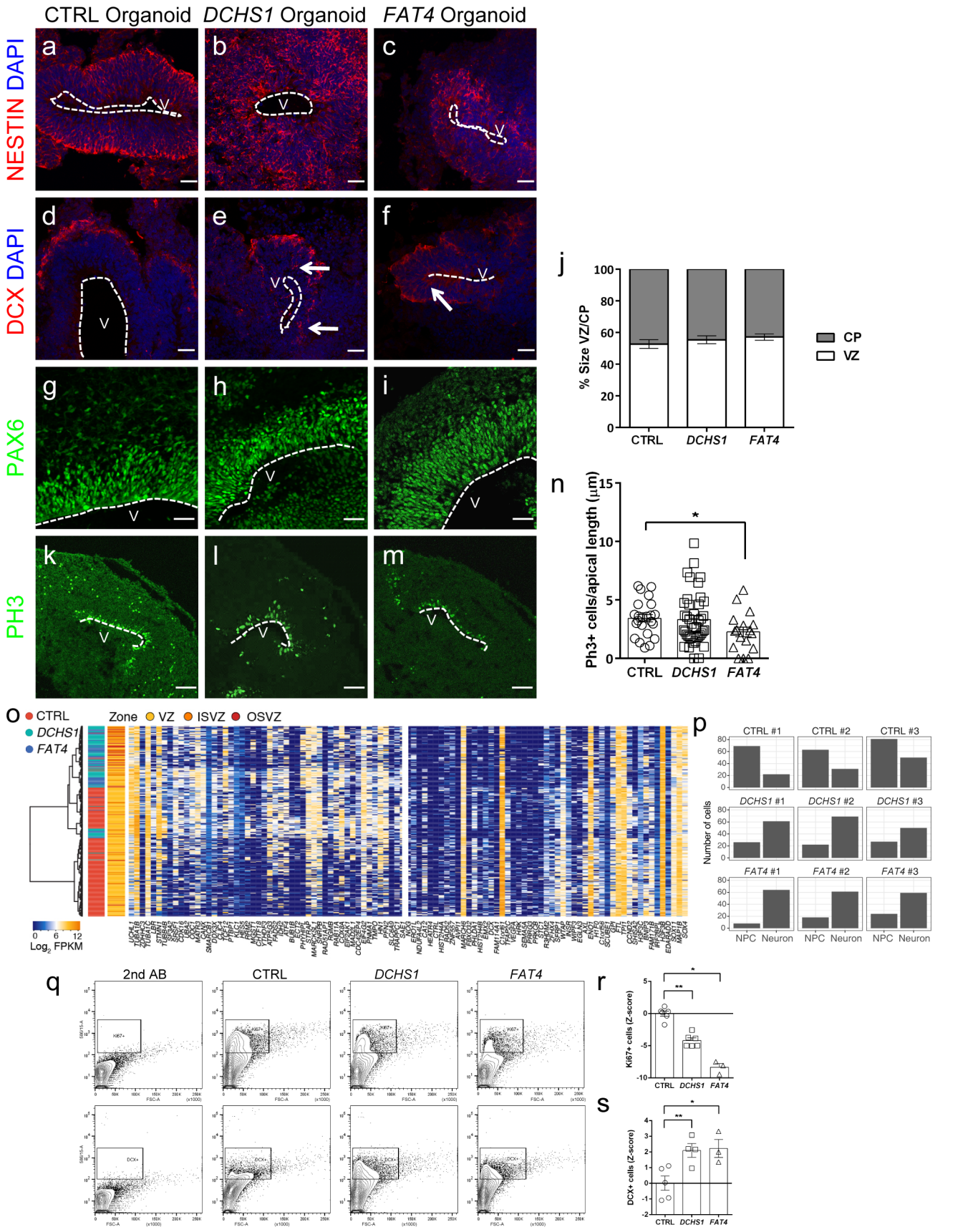

Extended Data Fig. 3 | See next page for figure caption.

Extended Data Fig. 3 | Neural progenitor proliferation and signatures in mutant organoids. a–i,k–m, Micrographs of sections of mutant cerebral organoids from day 20 immunostained for NESTIN (**a–c**) and DCX (**d–f**) and from day 42 immunostained for PAX6 (**g–i**) and PH3 (**k–m**). **a–f**, $b = 1$, $o = 3$ per condition; **g–i**,**k–m**, $b = 3$, $o = 9$ per condition. **j**, Quantification of thickness of ventricular zone (VZ) and cortical plate (CP) structures in cerebral organoids ($v = 6$ CTRL, 11 *DCHS1*, 12 *FAT4*). **n**, Quantification of PH3+ cells per length of apical surface ($o = 3$, $v = 23$ CTRL, 41 *DCHS1*, 17 *FAT4*, $F_{(2,80)} = 2.41$, $P = 0.097$, comparison between CTRL and *FAT4* $F_{(1,39)} = 5.18$, $P = 0.029$). **o**, Hierarchical clustering visualizing for all NPCs (338 single cells), expression of genes identified by PCA (top 50 positively and negatively correlating with PC 1) on all NPCs. **p**, Number of NPCs and neurons for each experiment shown in **o**. **q**, FACS plots depicting the definition of the sorting gates (secondary antibodies control) and sorting of KI67+ or DCX+ cells in control, *DCHS1*- and *FAT4*-mutant organoids ($b = 2$, $o = 6$ CTRL, 6 *DCHS1*, 3 *FAT4*). **r**,**s**, *Z* scores of the quantification of KI67+ cells (**r**) and DCX+ cells (**s**) from FACs analysis shown in **q**. Statistical analysis was performed using two-tailed Mann Whitney test. **r**, CTRL to *DCHS1* $P = 0.0022$, CTRL to *FAT4* $P = 0.0238$. **s**, CTRL to *DCHS1* $P = 0.0317$, CTRL to *FAT4* $P = 0.0357$. Results are mean ± s.e.m. (**j**,**n**) or *z* scores as mean ± s.e.m. (**r**,**s**). Dotted lines highlight ventricles (V). Scale bars, 30 µm for **a–f** and 50 µm for **g–m**.

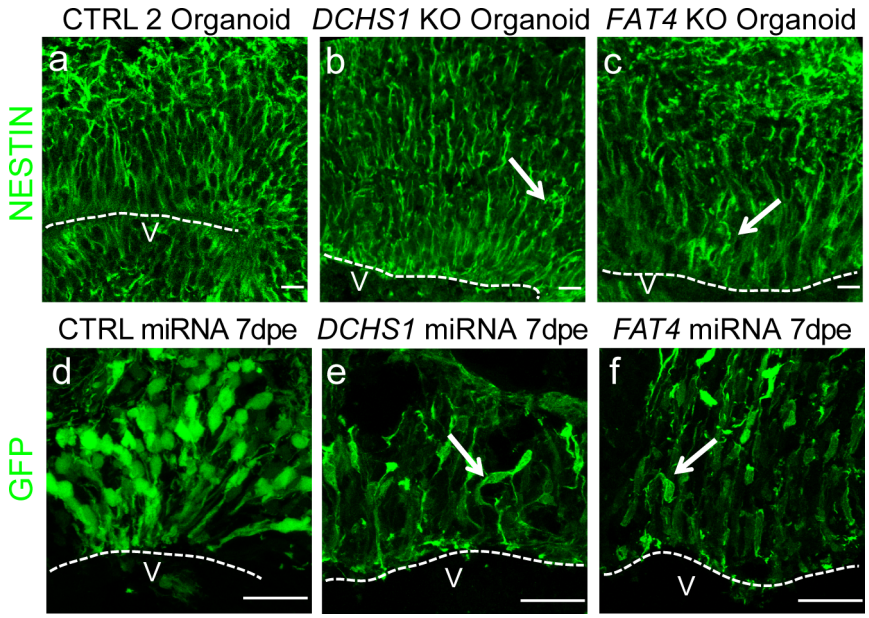

Extended Data Fig. 4 | Morphological changes in the NPCs upon *DCHS1* and *FAT4* deletion. a–**c**, Micrographs of sections of KO cerebral organoids day 40 immunostained for NESTIN. Arrows indicate the disrupted morphology of NPCs (**b**,**c**). **d**–**f**, Micrographs of sections of control organoids electroporated with miRNA against *DCHS1* or *FAT4* at day 42 and analyzed at day 49. Arrows indicate the disrupted morphology upon downregulation of *DCHS1* and *FAT4* (**e**,**f**). **a**–**c**, $b = 2$, $o = 6$ per condition; **d**–**f**, $b = 2$, $o = 6$ per condition. Dotted lines highlight ventricles (V). Scale bars, 30 μm.

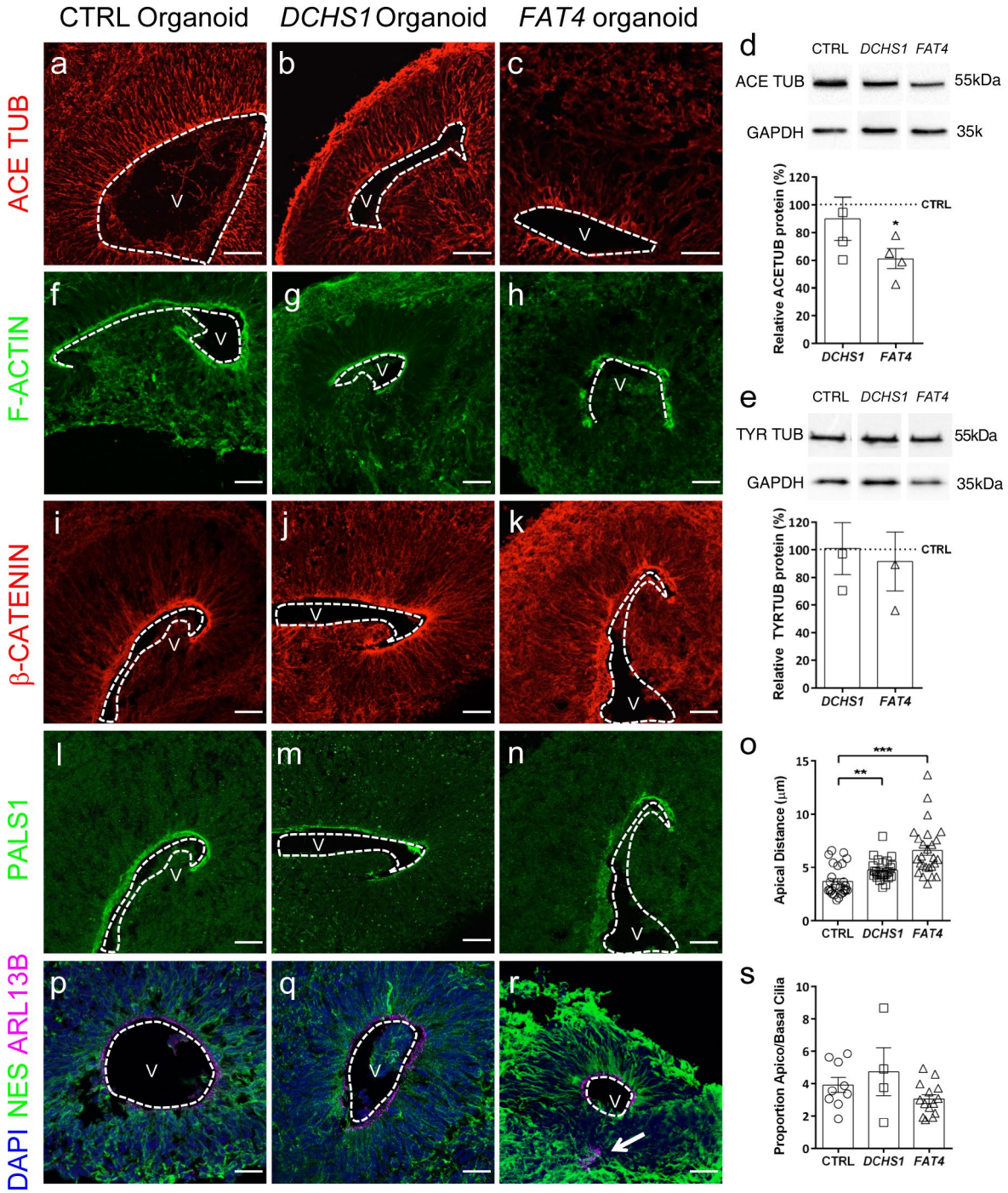

Extended Data Fig. 5 | Apicobasal polarity in cerebral organoids. a–**c**, Micrographs of sections of organoids (day 42) immunostained for ACETYLATED TUBULIN, $b = 2$, $o = 6$ per condition. **d**,**e**, Western blot and quantification of ACETYLATED TUBULIN (**d**) (independent cultures = 5 CTRL, 4 *DCHS1*, 4 *FAT4*, significance based on one sample two-tailed *t* test, $P = 0.562$ CTRL vs *DCHS1*, $P = 0.013$ CTRL vs *FAT4*) and TYROSINATED TUBULIN (**e**) (independent cultures = 3 CTRL, 3 *DCHS1*, 3 *FAT4*) levels in NPCs, significance based on one sample two-tailed *t* test, $P = 0.967$ CTRL vs *DCHS1*, $P = 0.728$ CTRL vs *FAT4*. **f**-**n**,**p**-**r**, Micrographs of sections of cerebral organoids (day 42) immunostained as indicated in the panels. **f**-**n**,**p**-**r**, $b = 3$, $o = 9$ per condition. **o**, Quantification of the distance from the apical surface (positive for β-CATENIN and PALS1) and DAPI+ nuclei of NPCs ($v = 27$ CTRL, 26 *DCHS1*, 26 *FAT4*; 5 different positions were measured and averaged for each ventricle; significance based on one-sample two-tailed *t* test, $P = 0.0025$ CTRL vs *DCHS1*, $P = 0.001$ CTRL vs *FAT4*). **s**, Ratio of ARL13B fluorescence intensity measured at the apical surface (cilia facing the ventricular lumen) and at basal position (all the rest of the cilia in the germinal and cortical zones) ($b = 5$, $o = 15$, $v = 9$ CTRL, 4 *DCHS1*, 14 *FAT4*, significance based on one-sample *t* test). Results are mean ± s.e.m. Dotted lines highlight ventricles (V). Scale bar, 50 μm (**a**-**c**) and 20 μm (**f**-**r**).

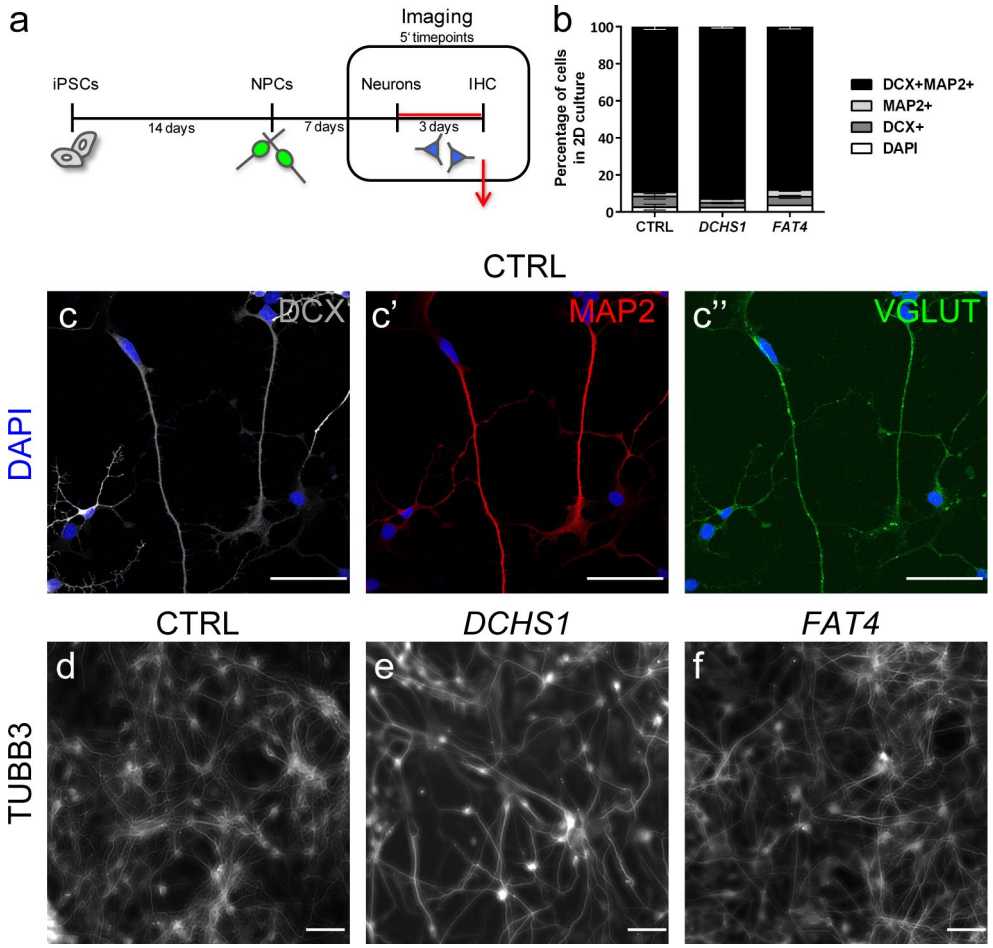

Extended Data Fig. 6 | 2D time-lapse imaging experimental design and morphological changes of mutant neurons. a, Experimental design for 2D live imaging of migrating neurons. Neural progenitors were differentiated for 7 d and imaged for 3 d every 5 min. **b**, Quantification of the percentage of cells expressing DCX, MAP2 or both markers in neuronal cultures after 10 d in culture. **c**–**c**″, Immunostaining for DoubleCortin (DCX), MAP2 (mature neurons) and VGLUT (glutamatergic neurons) in 2D neurons derived from control cells in monolayer culture, $b = 3$, independent cultures = 9 per condition. **d**–**f**, Immunostaining for TUBB3 in 2D neurons derived from control and mutant cells in monolayer culture, $b = 3$, independent cultures = 9 per condition. Results are mean ± s.e.m. Scale bar, 20 μm.

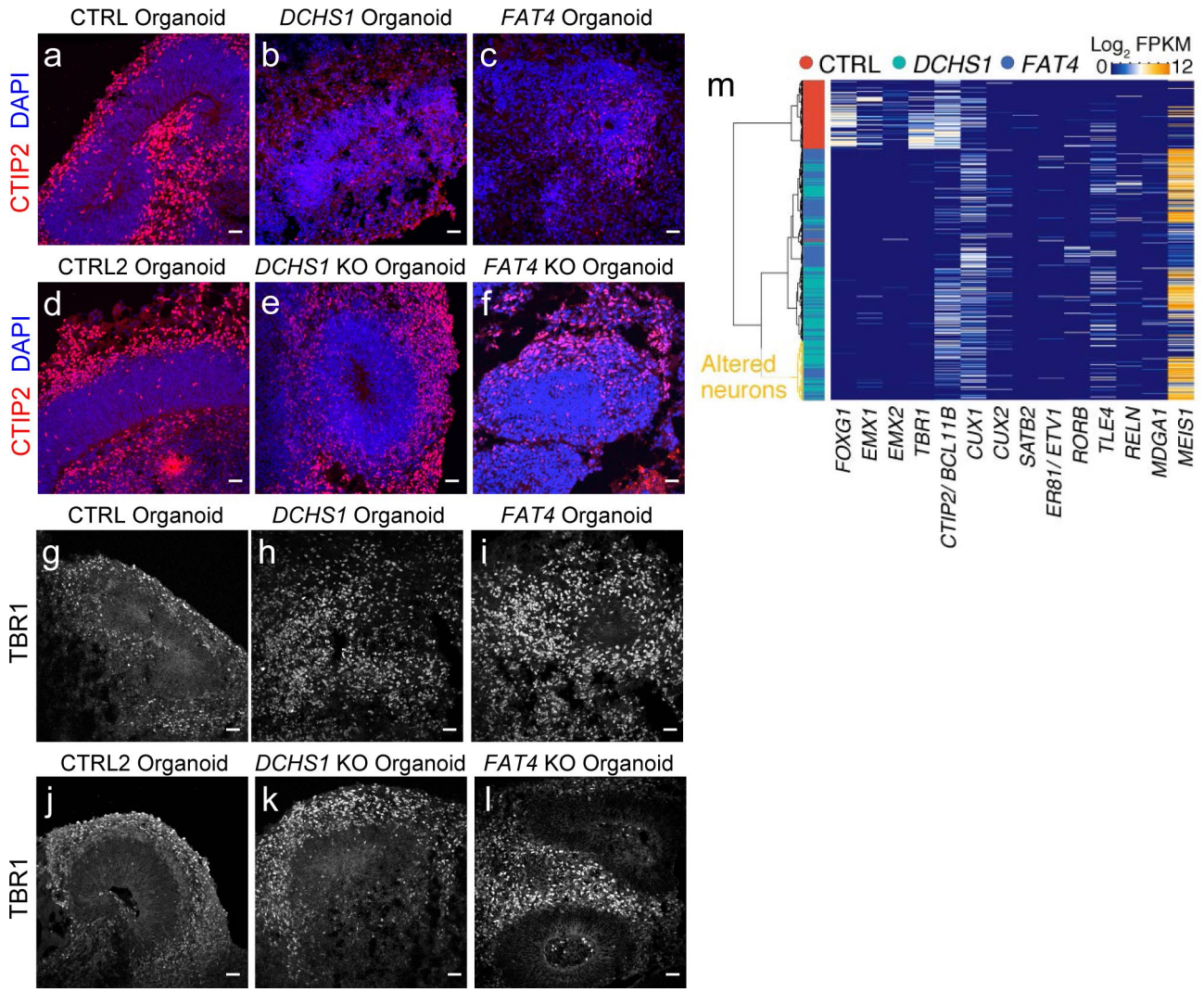

Extended Data Fig. 7 | Characterization of mutant and KO organoid regions. a–l, Micrographs of sections of mutant and KO organoids immunostained as depicted in the panels. **a–c**,**g–i**, $b = 3$, $o = 9$ per condition; **d–f**,**j–l**, $b = 2$, $o = 6$ per condition. **m**, Heat map showing expression of genes marking neurons in the cortex/forebrain (columns) for all neuronal cells from control and mutant organoids (rows, 467 single cells). Scale bar, 30 μm.

nature research

Corresponding author(s): Silvia Cappello and Barbara Treutlein

Life Sciences Reporting Summary

Nature Research wishes to improve the reproducibility of the work that we publish. This form is intended for publication with all accepted life science papers and provides structure for consistency and transparency in reporting. Every life science submission will use this form; some list items might not apply to an individual manuscript, but all fields must be completed for clarity.

For further information on the points included in this form, see Reporting Life Sciences Research. For further information on Nature Research policies, including our data availability policy, see Authors & Referees and the Editorial Policy Checklist.

Please do not complete any field with "not applicable" or n/a. Refer to the help text for what text to use if an item is not relevant to your study.

For final submission: please carefully check your responses for accuracy; you will not be able to make changes later.

Experimental design

1. Sample size

Describe how sample size was determined.

The disease investigated, Periventricular Heterotopia due to FAT4 or DCHS1 mutations, is a rare disease. We have very limited number of patients, therefore we used 2 different controls and 2 different patients cell lines. In order to compensate for the limited number of patient's cells we generated isogenic FAT4 and DCHS1 KO iPSC lines form a third CTRL line.

2. Data exclusions

Describe any data exclusions.

All data are included

3. Replication

Describe the measures taken to verify the reproducibility of the experimental findings.

All experiments were reproduced at least 3 times independently and all attempts at replication were successful.

4. Randomization

Describe how samples/organisms/participants were allocated into experimental groups.

We do not have experimental groups, only 2 patients were available.

5. Blinding

Describe whether the investigators were blinded to group allocation during data collection and/or analysis.

In the first submission, the majority of the data were acquired in a non-blinded manner. The investigator was aware of the genotypes. All data acquired were after controlled by a second person to confirm the results. While revising the manuscript, as suggested, the investigators were blinded and all data were confirmed.

Note: all in vivo studies must report how sample size was determined and whether blinding and randomization were used.

6. Statistical parameters

For all figures and tables that use statistical methods, confirm that the following items are present in relevant figure legends (or in the Methods section if additional space is needed).

n/a	Confirmed
☐	☒ The exact sample size (*n*) for each experimental group/condition, given as a discrete number and unit of measurement (animals, litters, cultures, etc.)
☐	☒ A description of how samples were collected, noting whether measurements were taken from distinct samples or whether the same sample was measured repeatedly
☐	☒ A statement indicating how many times each experiment was replicated
☐	☒ The statistical test(s) used and whether they are one- or two-sided *Only common tests should be described solely by name; describe more complex techniques in the Methods section.*
☐	☒ A description of any assumptions or corrections, such as an adjustment for multiple comparisons
☐	☒ Test values indicating whether an effect is present *Provide confidence intervals or give results of significance tests (e.g. P values) as exact values whenever appropriate and with effect sizes noted.*
☐	☒ A clear description of statistics including central tendency (e.g. median, mean) and variation (e.g. standard deviation, interquartile range)
☐	☒ Clearly defined error bars in all relevant figure captions (with explicit mention of central tendency and variation)

See the web collection on statistics for biologists for further resources and guidance.

Software

Policy information about availability of computer code

7. Software

Describe the software used to analyze the data in this study.	ImageJ; GraphPad Prism, Seurat v 2.3.0, Monocle2 v2.0.0/ v 2.6.3, TopHat, Genomics Cell Ranger software v 2.1.0, SAMtools, R studio The packages/ software that we used are open source/ code is available. (Custom code such as analysis scripts could be made available upon request).

For manuscripts utilizing custom algorithms or software that are central to the paper but not yet described in the published literature, software must be made available to editors and reviewers upon request. We strongly encourage code deposition in a community repository (e.g. GitHub). *Nature Methods* guidance for providing algorithms and software for publication provides further information on this topic.

Materials and reagents

Policy information about availability of materials

8. Materials availability

Indicate whether there are restrictions on availability of unique materials or if these materials are only available for distribution by a third party.	Only samples derived from patients are restricted

9. Antibodies

Describe the antibodies used and how they were validated for use in the system under study (i.e. assay and species).	All antibodies are commercially available antibodies commonly used is several other publications. Every antibody was then validated in the lab to exclude non-specific signals due to secondary antibodies. Antigen Dilution Vendor Catalog # Clone name Lot number PAX6 1:500 Biolegend PRB-278p Poly19013 B244513 MAP2 1:500 Sigma Aldrich M4403 HM-2, monoclonal 035MN4780V TUBB3 1:500 Sigma Aldrich T8660 SDL.3D10, monoclonal 103M4830 NESTIN 1:200 Millipore MAB5326 clone 10C2 3112610 TYROSINATE TUBULIN 1:1000 Merck Millipore ABT171 YL1/2 - ACETYLATED TUBULIN 1:6000 Sigma Aldrich T7451 6-11B-1, monoclonal 025M4757 PALS1 1:500 Sigma Aldrich 07-708 - H0907 β-CATENIN 1:500 BD Biosciences 610154 14/Beta-Catenin 76645 PH3 1:500 Millipore 06-570 - 3113883 ARL13B 1:200 Proteintech 17711-1-AP - - GAPDH 1:6000 Millipore CB1001 6C5 2896484 GFP 1:1000 Aves Lab GFP-1020 - 697986 PHALLOIDIN (ACTIN) 1:40 Thermo Fisher A12381 - - DoubleCortin (DCX) 1:2000 Millipore AB2253 - 2787730 VGLUT 1:500 SY SY 135403 - - NEUN 1:500 Millipore MAB377 clone A60 2742283 KI67 1:500 DAKO M7248 Clone MIB-5 20017551 Tbr1 1:500 Abcam Ab31940 - GR3217067-1 CTIP2 1:500 Abcam Ab18465 25B6 GR322373-4

10. Eukaryotic cell lines

a. State the source of each eukaryotic cell line used.	Patients fibroblasts and one control line were provided by Dr. Stephen Roberson (author).Commercially available control fibroblasts were included in this study (ATCC and NuFF3-RQ).
b. Describe the method of cell line authentication used.	Each patient line has been genotyped (Cappello et al., Nature Genetics 2013). Both commercially available lines and were karyotyped. FAT4 KO and DCHS1 KO were karyotyped.
c. Report whether the cell lines were tested for mycoplasma contamination.	All cells were tested for mycoplasma monthly and always resulted negative.
d. If any of the cell lines used are listed in the database of commonly misidentified cell lines maintained by ICLAC, provide a scientific rationale for their use.	No commonly misidentified cell lines were used

Animals and human research participants

Policy information about studies involving animals; when reporting animal research, follow the ARRIVE guidelines

11. Description of research animals

Provide all relevant details on animals and/or animal-derived materials used in the study.	The study did not involve research animals.

Policy information about studies involving human research participants

12. Description of human research participants

Describe the covariate-relevant population characteristics of the human research participants.	All IPS cells were derived from fibroblasts of males between 0 and 12 (CTRL 1: newborn; CTRL2 and KOs: 7 years; DCHS1: 7 years; FAT4: 12 years)